Univerzita Karlova v Praze

Přírodovědecká Fakulta

Katedra Fyziologie

Bc. Martin Valný

NMDA receptory u astrocytů: jejich funkce v ischemicky poškozené nervové tkáni

NMDA receptors in astrocytes: their role in ischemic brain injury

Diplomová práce

Vedoucí práce: Ing. Miroslava Anděrová, CSc.

Praha, 2013

Prohlašuji, že jsem závěrečnou práci zpracoval samostatně a že jsem uvedl všechny použité informační zdroje a literaturu. Tato práce ani její podstatná část nebyla předložena k získání jiného nebo stejného akademického titulu.

V Praze 2.5.2013

……

Rád bych na tomto místě poděkoval své školitelce Ing. Miroslavě Anděrové, CSc. za odborné vedení, trpělivost a shovívavost. Dále bych chtěl poděkovat Mgr. Dávidu Džambovi za cenné rady a pomoc při práci v laboratoři a Ing. Vendule Rusňákové za spolupráci při analýze genové exprese.

ABSTRACT

Glutamate is the main excitatory neurotransmitter in the mammalian brain, and its transmission is responsible for higher brain functions, such as learning, memory and cognition. Glutamate action is mediated by variety of glutamate receptors, of which N-methyl-D-aspartate (NMDA) receptors are the most remarkable due to their high Ca^{2+} permeability and complex pharmacology. Despite the widespread expression of NMDA receptors in astroglial cells in different brain regions, they have been studied mostly in neurons. Therefore, the role of astroglial NMDA receptors under physiological conditions as well as in pathological states, such as cerebral ischemia, is not fully understood. The aim of this work was to elucidate the presence, composition and function of these receptors in astrocytes under physiological conditions and after focal cerebral ischemia. For this purpose, we used transgenic (GFAP/EGFP) mice, in which astrocytes express enhanced green fluorescent protein (EGFP) under the control of human promotor for glial fibrillary acidic protein (GFAP) enabling astrocyte isolation and their collection via fluorescence-activated cell sorting. We performed single-cell RT-qPCR analysis of astrocytes isolated from the cortex of adult mice. The analyzed cells were isolated from the uninjured brains of 50 days old mice (control) and mice 3, 7 and 14 days after middle cerebral artery occlusion (MCAo), a model of ischemic injury. For each cell, we analyzed the expression of genes specific for astrocytes, reactive astrocytes and individual subunits of NMDA receptors. Additionally, we have employed immunohistochemical analysis and intracellular Ca^{2+}-imaging technique to elucidate the functional properties of astroglial NMDA receptors. Gene expression profiling revealed that astrocytes express genes for all NMDA receptor subunits, of which expression was increased after ischemic injury. Nevertheless, our immunohistochemical analysis showed that astrocytes express only GluN1, GluN2C, GluN2D and GluN3A subunits. Furthermore, intracellular

Ca^{2+}-imaging disclosed that under physiological conditions the activation of astroglial NMDA receptors results in significant Ca^{2+} entry into the cell, while under ischemic conditions the Ca^{2+} permeability of astroglial NMDA receptors is markedly reduced. Based on our findings, we conclude that astroglial NMDA receptors probably do not contribute to Ca^{2+}-mediated cell damage following ischemic injury.

ABSTRAKT

Glutamát je hlavní excitační neuropřenašeč v mozku savců a je zodpovědný za vyšší mozkové funkce jako jsou učení, paměť či kognice. Účinek glutamátu je zprostředkován různými typy glutamátových receptorů, z nichž nejvíce pozornosti poutají N-methyl-D-aspartát (NMDA) receptory disponující vysokou propustností pro vápník a složitou farmakologií. Navzdory tomu, že jsou NMDA receptory hojně exprimovány v astrocytech různých oblastí mozku, doposud byly studovány především ve spojitosti s neuronální aktivitou, což je důvod, proč jejich úloha jak ve zdravém, tak i v poškozeném mozku zůstává neobjasněna. Cílem této práce bylo studovat NMDA receptory v astrocytech za fyziologických podmínek a identifikovat změny v jejich složení a funkci po fokální mozkové ischemii. Za tímto účelem byly použity transgenní myši (GFAP/EGFP), u kterých jsou astrocyty označeny zeleným fluorescenčním proteinem (EGFP), který je exprimován pod lidským promotorem pro gliální fibrilární acidický protein (GFAP). Použití těchto myší umožnilo izolaci EGFP-pozitivních astrocytů pomocí fluorescenční průtokové cytometrie. Byla provedena RT-qPCR analýza jednotlivých astrocytů, které byly izolovány z mozkové kůry neporaněných, 50 dní starých myší (kontrola) a myší 3, 7 a 14 dní po okluzi střední mozkové tepny, model fokální mozkové ischemie. Každá buňka byla testována na expresi genů kódujících specifické markery astrocytů, reaktivních astrocytů a genů kódujících jednotlivé podjednotky NMDA receptorů. Následně byla provedena

imunohistochemická analýza a pomocí techniky fluorescenčního zobrazování intracelulárních hladin vápníku byly studovány funkční vlastnosti astrogliálních NMDA receptorů. Ačkoliv analýza genové exprese ukázala, že astrocyty exprimují geny všech podjednotek NMDA receptorů a že jejich exprese vzrůstá po ischemickém poškození, imunohistochemicky byly detekovány pouze podjednotky GluN1, GluN2C, GluN2D a GluN3A. Výsledky fluorescenčního zobrazování hladin intracelulárního vápníku ukázaly, že za fyziologických podmínek vede aktivace astrogliálních NMDA receptorů ke vtoku vápníku do astrocytů, zatímco za ischemických podmínek je propustnost astrogliálních receptorů pro vápník výrazně snížena. Na základě uvedených výsledků můžeme uzavřít, že astrogliální NMDA receptory po ischemii pravděpodobně nepřispívají k vápníkem vyvolanému poškození astrocytů.

CONTENTS

LIST OF ABBREVIATION

$[Ca^{2+}]_I$	intracellular calcium concentration
$[Glu]_o$	extracellular glutamate concentration
$[K^+]_o$	extracellular potassium concentration
$[Na^+]_o$	extracellular sodium concentration
ABD	agonist-binding domain
aCSF	artificial cerebrospinal fluid
AMPA	α-amino-3-hydroxy-5-methyl-4-isoxazolepropionic acid
AQP4	aquaporin 4
ATP	adenosine triphosphate
BLAST	basic local alignment search tool
CA1	Cornu Ammonis 1
$CaCl_2$	calcium chloride
cDNA	clone deoxyribonucleic acid
CDs	current densities
C_m	membrane capacitance
CNS	central nervous system
C_q	quantification cycle
CREB	cyclic-adenosin monophosphate response element-binding protein
Cspg4	chondroitin sulfate proteoglycan 4
CTRL	control
D3-14	day 3-14 after middle cerebral artery occlusion
Da	Dalton
D-AP-5	D-2-amino-5-phosphonopentanoic acid
DNA	deoxyribonucleic acid
dNTP	deoxyribonucleotide triphosphate
EAAT	excitatory amino acid transporter

EGFP	enhanced green fluorescent protein
$EGFP^+$	enhanced green fluorescent protein positive
F	fluorescence intensity
FBS	fetal bovine serum
GABA	γ-aminobutyric acid
$GABA_A$	γ-aminobutyric acid receptor A
GFAP	glial fibrillary acidic protein
GFAP	gene coding glial fibrillary acidic protein
GLAST	glutamate/aspartate transporter
Gln	glutamine
GLT-1	glutamate transporter 1
Glu	glutamate
Glul	gene coding glutamine synthase
GluN	subunit of NMDA receptor
GluR	glutamate receptors
Grin	genes coding NMDA receptors subunits
HEPES	4-(2-hydroxyethyl)-1-piperazineethanesulfonic acid
i.d.	inner diameter
i.p.	intra-peritoneally
iGluRs	ionotropic glutamate receptors
$InsP_3$	inositol-3-phosphate
K_a	fast activating and inactivating outwardly rectifying K^+ current
KCl	potassium chloride
K_{dr}	voltage-gated delayed outwardly rectifying K^+ current
K_{ir}	inwardly rectifying K^+ current
Kir4.1	inwardly rectifying K^+ channels 4.1
MCA	middle cerebral artery
MCAo	middle cerebral artery occlusion

Mg-ATP	magnesium adenosine triphosphate
$MgCl_2$	magnesium chloride
mGluR	metabotropic glutamate receptor
MK-801	Dizocilpine
Na_2HPO_4	disodium hydrogen phosphate
NaCl	natrium chloride
$NaHCO_3$	sodium bicarbonate
NCBI	national center for biotechnology information
NCX	sodium/calcium exchanger
NF-κB	nuclear factor kappa-light-chain-enhancer of activated B cells
NG2	neuron-glial antigen 2
NMDA	N-methyl-D-aspartate
NMDG	N-methyl-D-glucamine
NTD	N-terminal domain
OGB1	Oregon Green BAPTA1
OGB1-AM	Oregon Green BAPTA1-acetoxymethyl ester
OGD	oxygen-glucose deprivation
$P_2X_{1/5}$	P_2X purinoreceptor 1/5
P_2X_7	P_2X purinoreceptor 7
Pdgfαr	gene coding platelet-derived growth factor α receptor
PTB	pentobarbital
qPCR	quantitative polymerase chain reaction
R_m	membrane resistance
RMP	resting membrane potential
RNA	ribonucleic acid
ROS	reactive oxygen species
RPM	rotate per minute
RT-PCR	reverse transcription - polymerase chain reaction

S.E.M.	standard error of the mean
Slc1a2	gene coding solute carrier family 1 member 2
TIDs	transient ischemic depolarizations
T_m	melting temperature
TTC	2,3,5-triphenyltetrazolium chloride
TTX	tetrodotoxin
UBP-141	(2R*,3S*)-1-(Phenanthrenyl-3-carbonyl)piperazine-2,3-dicarboxylic acid
Vim	gene coding vimentin
V_m	membrane potential
VRACs	volume-regulated anion channels

INTRODUCTION

Cerebral ischemia, clinically defined as loss of brain function due to death of neurons, is the fourth leading cause of death and long-term disability in civilized countries (Hoyert and Xu, 2012). Cerebral ischemia results from cardiac arrest or occlusion of one of the major brain arteries (stroke). Such conditions lead to reduced blood supply and in turn to pathophysiological changes that underlie brain damage. Despite high incidence of cerebral ischemia, the only effective strategy used to combat its consequences is re-establishment of blood supply by thrombolysis in the case of stroke, or by resuscitation in the case of heart failure (Blakeley and Llinas, 2007). Therefore many studies are focused on cellular mechanisms of ischemic brain damage.

Since cerebral ischemia results in extensive neuronal death, beginnings of hunt for cellular basis of cerebral ischemia were primarily focused on neurons. Many clinical trials were based on neuroprotective strategies, such as administration of glutamate receptor antagonists or blockers of voltage-gated Na^+ and Ca^{2+} channels, however they were not successful (Danton and Dietrich, 2004). Since neurocentric view of central nervous system (CNS) was extended by glial cells in last decades, the attention is not only focused on neuronal, but also on non-neuronal mechanisms that underlie cerebral ischemia (Nedergaard and Dirnagl, 2005). Glial cells play essential role in CNS including K^+ buffering, glutamate clearance, metabolic support of neurons or modulation of synaptic transmission. As all these processes are impaired in pathophysiology of cerebral ischemia, glial cells represent an excellent therapeutic target to improve outcome following cerebral ischemia.

Ischemia-induced cellular damage is mediated predominantly by excessive accumulation of glutamate in extracellular space, which leads to the increase in intracellular Ca^{2+} concentration. Calcium overload triggers number of events such as degradation of vital molecules, mitochondrial damage or reactive

oxygen species (ROS) production ultimately resulting in cell death (Won et al., 2002). Calcium influx may also be a result of activation of NMDA receptors (glutamate-gated ion channels), which were considered as exclusively neuronal for a long time. However, recent studies showed presence of NMDA receptors also in glial cells. One of the unresolved questions therefore remains, what is the role of these glial NMDA receptors in pathophysiology of cerebral ischemia.

1 GLIAL CELLS

Glial cells are non-neuronal cells that provide support and protection for neurons in the CNS. Today we distinguish five main types of glial cells: Astrocytes, oligodendrocytes, ependymal cells, NG2-glia and microglia. Oligodendrocytes are glial cells with a few parallel processes and their function is the production of myelin, which insulates axons in the CNS and hence provides for fast action potential propagation. Ependymal cells form the walls of the ventricles in the brain and the central canal of spinal cord and are involved in the production and movement of cerebrospinal fluid. Microglial cells originate from macrophages that invade the brain during early development and represent the immune system of the brain. The fourth type of glial cells are neuron-glial antigen 2 (NG2) proteoglycan expressing glia. They were characterized recently and their function in the brain is not fully elucidated, however it is believed that NG2-glia are multipotent adult neural progenitor cells, which can give rise to oligodendrocytes, astrocytes and potentially, to neurons. The largest and functionally most important class of glial cells is represented by astrocytes (Verkhratsky and Butt, 2007).

2 General physiology of astrocytes

Astrocytes or astroglia were for a long time considered as connective tissue that holds neurons together. Discoveries of the last decades proved many other astrocytic functions in the CNS, such as structural and metabolic support of neurons, maintenance of ionic and neurotransmitter homeostasis and active participation in information processing. Although large progress in understanding of astroglial function was made during last three decades, many aspects of astroglial (patho)physiology remain still unresolved.

2.1 Morphology

Astrocytes are the most numerous group of glial cells represented by many subtypes, which differ in their morphology, physiology and location. Typical morphological feature of astrocytes is expression of glial fibrillary acidic protein (GFAP), which is frequently used as astroglial marker; however, its expression varies between different astroglial subtypes. For example GFAP is expressed by almost all Bergmann glia, but only 10-25 % of astrocytes in cortex and hippocampus express GFAP. Although many morphological types of astrocytes were described, the largest "classical" group comprises star-like protoplasmic and fibrous astrocytes (**Fig. 1**) (Emsley and Macklis, 2006).

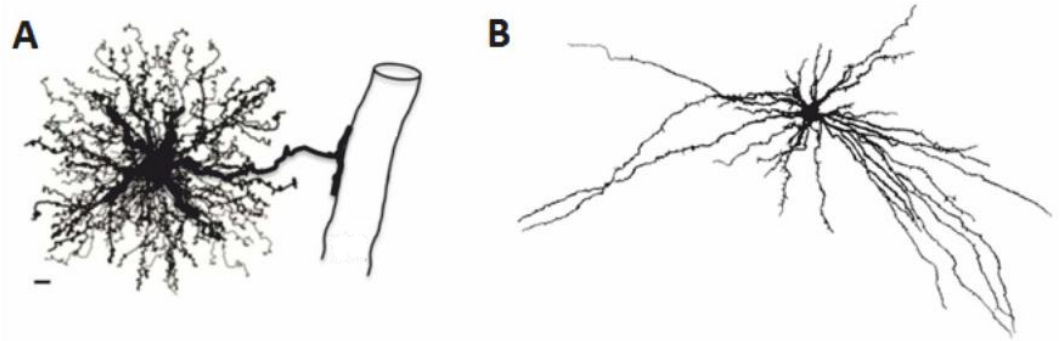

Figure 1. Protoplasmic and fibrous astrocytes. A) Processes of protoplasmic astrocyte form dense network that contacts neurons and blood vessels and they are found mainly in grey matter (scale bar 3 µM)(Sofroniew and Vinters, 2010). **B)** Fibrous astrocytes with many long processes are found in white matter (Cannon, 1985).

Protoplasmic astrocytes are found in gray matter and are endowed with many complex bushy processes that form contacts with blood vessels via perivascular endfeet and cover large number of neuronal synapses within their region. Fibrous astrocytes have many long (up to 300 µm) fiber-like processes that form several perivascular and subpial contacts. In contrast to protoplasmic astrocytes, fibrous astrocytes are found mainly in the white matter, where they form contacts with nodes of Ranvier by perinodal processes (Verkhratsky and Butt, 2007). The second large group of astroglial cells is represented by radial glia. Radial glial cell is usually formed by two main processes, one of them contacting ventricles and the second reaching pial membrane. There are two main subtypes of radial glia in adult CNS: the cerebellar Bergman glia and retinal Müller glia (Verkhratsky and Butt, 2007).

2.2 Brain microstructure

Astrocytes divide grey matter into relatively independent structural microdomains defined by astroglial branching. Within these territories astrocytes form multiple contacts with nearby neurons and blood vessels. For example, one astrocyte can contact 4 to 8 neurons and surround approximately 300-600 dendrites in adult mouse cortex (Halassa et al., 2007). In rat CA1 region of the hippocampus one astrocyte is estimated to enwrap around 140 000 synapses (Bushong et al., 2002). These discrete astroglial domains are further integrated into astroglial syncytium by gap junctions that form direct intercellular contacts between astrocytes (**Fig. 2**). Within this syncytium, long-range inter-glial communication allows many molecules like second messengers inositol-3-phosphate ($InsP_3$) and Ca^{2+} to diffuse from one cell to another. Diffusion of $InsP_3$ and consequent release of Ca^{2+} from endoplasmic reticulum is considered to be substrate for astroglial excitability, which is manifested as propagating Ca^{2+} wave (Scemes and Giaume, 2006). It should be mentioned that human astrocytes are far more complex than astrocytes in rodents. Protoplasmic astrocytes in human

cortex are 2.6-times larger in diameter and extend 10-times more primary processes than their rodent counterparts. This leads to much larger space occupied by single astrocyte in human brain, where it can cover up to two million of synapses (Oberheim et al., 2009).

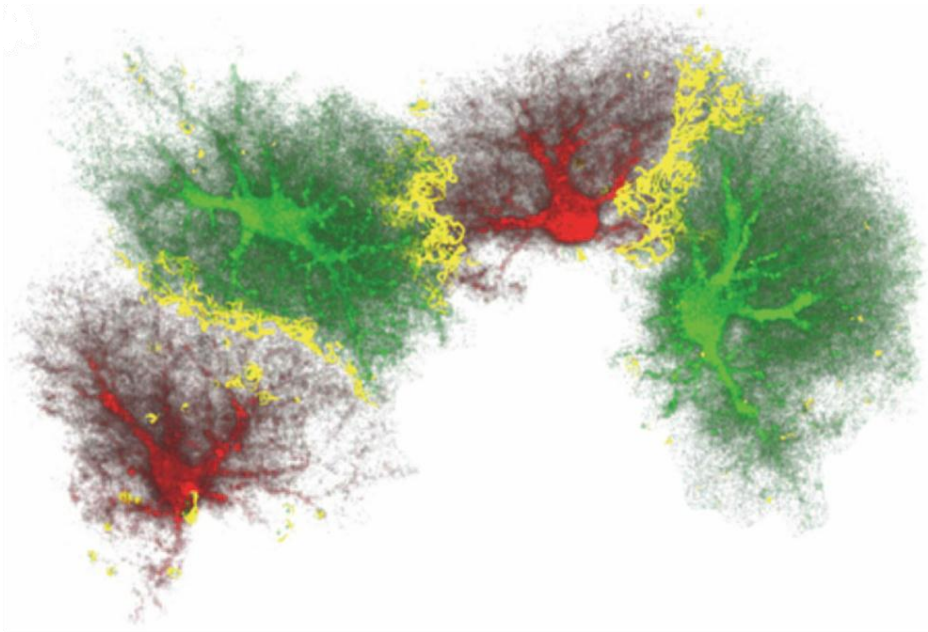

Figure 2. Astroglial microdomains. 3-dimensional reconstruction of astroglial microdomains in dentate gyrus. The yellow zone shows the border area where cellular processes of two adjacent astrocytes interdigitate (Wilhelmsson et al., 2006).

2.3 Metabolism

As astrocytes form functional link between neurons and blood vessels, they provide integration of neuronal circuitry with local blood flow. The phenomenon of rapid vasodilation triggered by focal increase in neuronal activity, known as functional hyperaemia, was observed already in 19th century by Roy and Sherrington (Roy and Sherrington, 1890). It is known that increase in neuronal activity triggers Ca^{2+}-dependent signals, which promote release of vasoactive substances from astroglial endfeet (Metea and Newman, 2006). Increase in neuronal activity is not accompanied only by release of vasomodulators, but also

induces activity-dependent metabolic support of neurons known as "neuronal-glial lactate shuttle". Vast majority of glutamate release during synaptic transmission is taken up by astrocytes in Na^+-dependent manner. Consequent increase of intracellular Na^+ concentration indirectly stimulates aerobic glycolysis, which results in production of lactate. Lactate is then transported to active neurons, where it is utilized for production of adenosine triphosphate (ATP) via tricarboxilic acid cycle (**Fig. 3**)

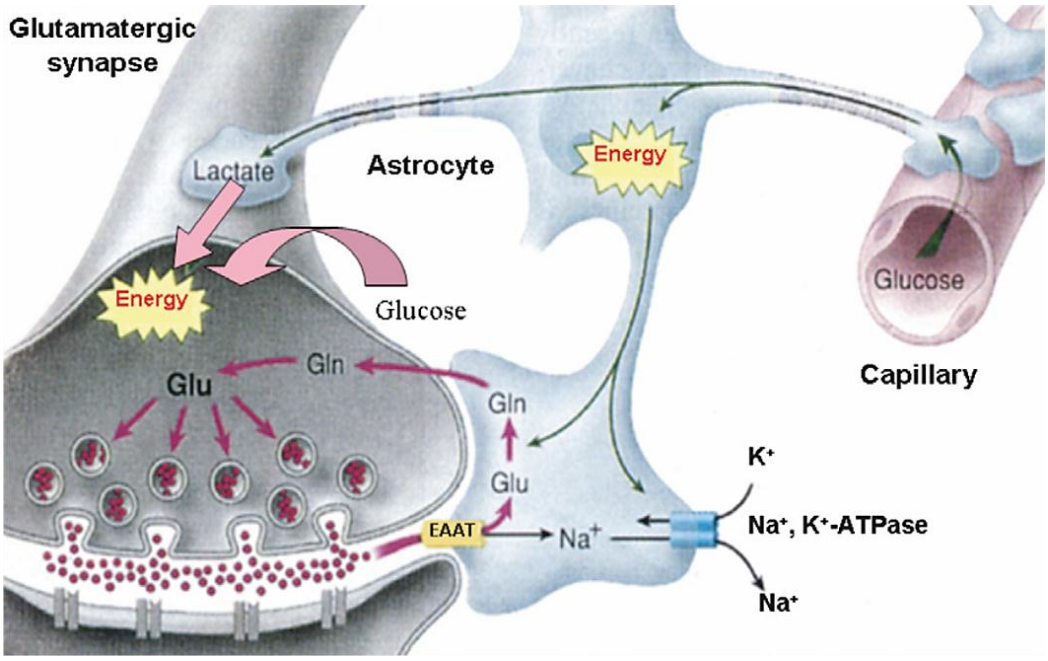

Figure 3. Model of neuronal-glial metabolic coupling. Glutamate released during synaptic action is taken up by Na^+-dependent co-transport to perisynaptic astroglial processes. Consequent increase in cytosolic Na^+ concentration stimulates lactate production. Lactate is then transported to neurons as energy substrate. Glu, glutamate; Gln, glutamine; EAAT, excitatory amino acid transporter (Magistretti, 2006)

Astrocytes not only support neurons by lactate, but they also serve as brain "energy stock", since they are almost exclusively able to store and handle glycogen in the CNS (Pellerin et al., 2007).

2.4 Maintenance of ionic and neurotransmitter homeostasis

Maintenance of extracellular homeostasis is necessary for proper brain function. Every synaptic action is accompanied by ionic redistribution, which profoundly affects membrane properties of neurons and therefore their excitability. Astrocytes, which express many transport systems that control extracellular levels of ions, neurotransmitters, water and other molecules, play a key role in keeping proper composition of extracellular fluid (for detail review see (Simard and Nedergaard, 2004)). Neuronal activity leads to transient local increases in extracellular K^+ concentration. Clearance of excessive K^+ is accomplished via local uptake predominantly mediated by astroglial Na^+/K^+-ATPases, $Na^+/K^+/2Cl^-$ co-transporter and inwardly rectifying K^+ channels 4.1 (Kir4.1). Kir4.1 channels also allow K^+ extrusion from astrocytes. The spatial K^+ buffering redistributes K^+ from areas with elevated K^+ concentration to regions with low extracellular concentration of K^+ and can occur within single astrocyte or within astroglial syncytium (**Fig. 4**) (Kofuji and Newman, 2004).

Redistribution of ions during synaptic action is accompanied by water movement to keep osmotic balance. Water homeostasis is accomplished also by astrocytes. Water enters and leaves astrocytes predominantly by water-permeable channels aquaporins 4 (AQP4), which are concentrated at perisynaptic, vascular and pial processes. Water and K^+ redistribution are tightly connected processes in such a way that alteration of water flux can impair K^+ buffering (Eid et al., 2005).

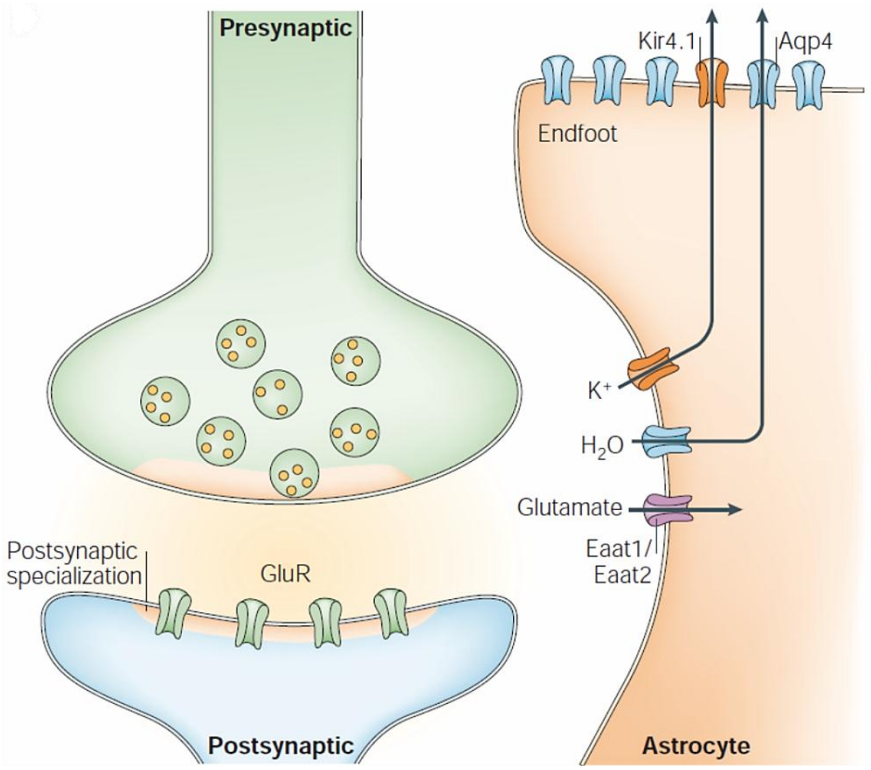

Figure 4. Scheme demonstrating astroglial homeostatic function. Excessive extracellular K^+ is taken up by various K^+ channels and transporters (Na^+/K^+-ATPases, $Na^+/K^+/2Cl^-$ co-transporter, Kir4.1) and together with water (via AQP4) are redistributed through astroglial syncytium (Amiry-Moghaddam and Ottersen, 2003). GluR, glutamate receptors; EAAT1/2, excitatory amino acid transporter 1/2; Kir4.1, inwardly rectifying K^+ channels 4.1; Aqp4, aquaporin 4.

Another essential role of astrocytes is removal of neurotransmitters, particularly glutamate, from synaptic cleft. Although glutamate is a major excitatory neurotransmitter, it is also one of the most potent neurotoxins and therefore prolonged presence of glutamate within synaptic cleft is highly undesirable (Won et al., 2002). Even though neurons are capable of re-uptake of released glutamate, the vast majority of glutamate is taken up by astrocytes. This transport is in human CNS accomplished by excitatory amino acid transporters EAAT1 and EAAT2 (in rodents known as glutamate/aspartate transporter, GLAST; and glutamate transporter 1, GLT1, respectively), which are expressed exclusively in astrocytes (**Fig. 5**). Moreover, astrocytes are involved in recovery of glutamate

to presynaptic terminals. After entering astroglial processes, glutamate is converted into glutamine by specific astroglial enzyme glutamine synthase. Non-toxic glutamine can be then transported to presynaptic buttons, where it is converted back into glutamate (McKenna, 2007)

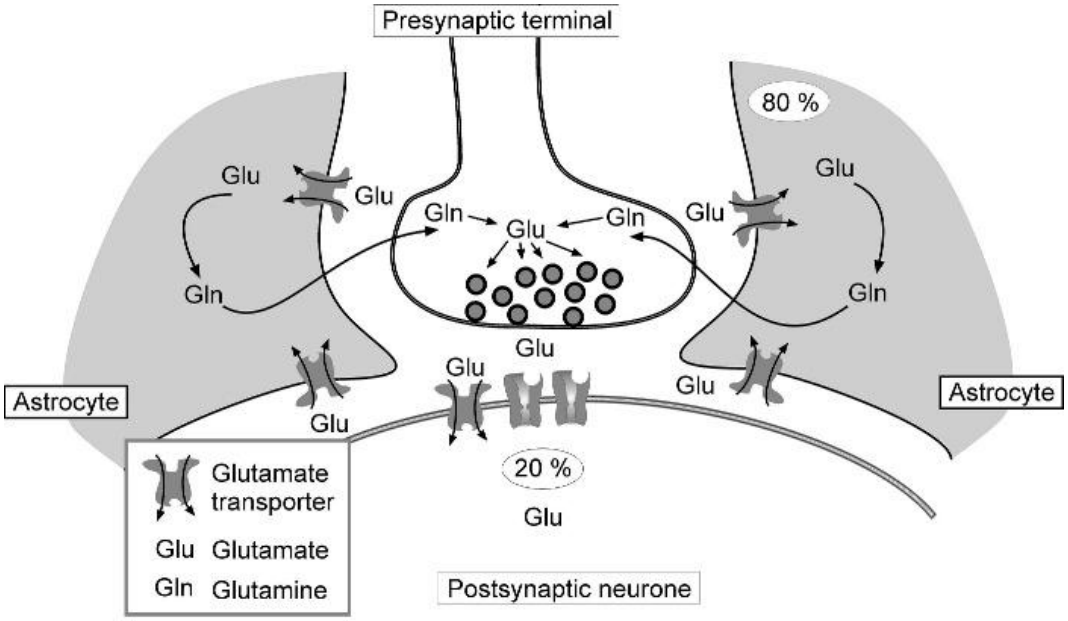

Figure 5. Glutamate uptake by glial and neuronal cells – the glutamate-glutamine cycle. Glutamate released during synaptic activity is removed from the synaptic cleft by glutamate transporters; about 80 percent of glutamate is accumulated by astrocytes and ~20 percent by postsynaptic neurons; presynaptic terminals do not accumulate glutamate. After entering the astrocyte, glutamate is converted into glutamine, which is then transported back to the presynaptic terminal, where it is converted into glutamate and accumulated into synaptic vesicles. This recycling of glutamate by astrocytes is known as the glutamate–glutamine cycle (Verkhratsky and Butt, 2007).

3 Astrocytes modulate neural circuitry

3.1 Gliotransmission

In addition to homeostatic function, astrocytes also contribute to information processing through modulation of synaptic transmission. Around

40% of all synapses in the brain are referred to exist as “tripartite synapses” (**Fig. 6**). In fact some synapses are enwrapped by astroglial processes, forming intimate structural relationship between these elements. Principally, astrocytes in tripartite synapse can sense synaptic transmission by numerous neurotransmitter receptors, which are expressed in astroglial membrane and furthermore, they can release gliotransmitters (e.g. glutamate, D-serine or ATP) and potentially modulate synaptic action (Araque et al., 1999; Ventura and Harris, 1999).

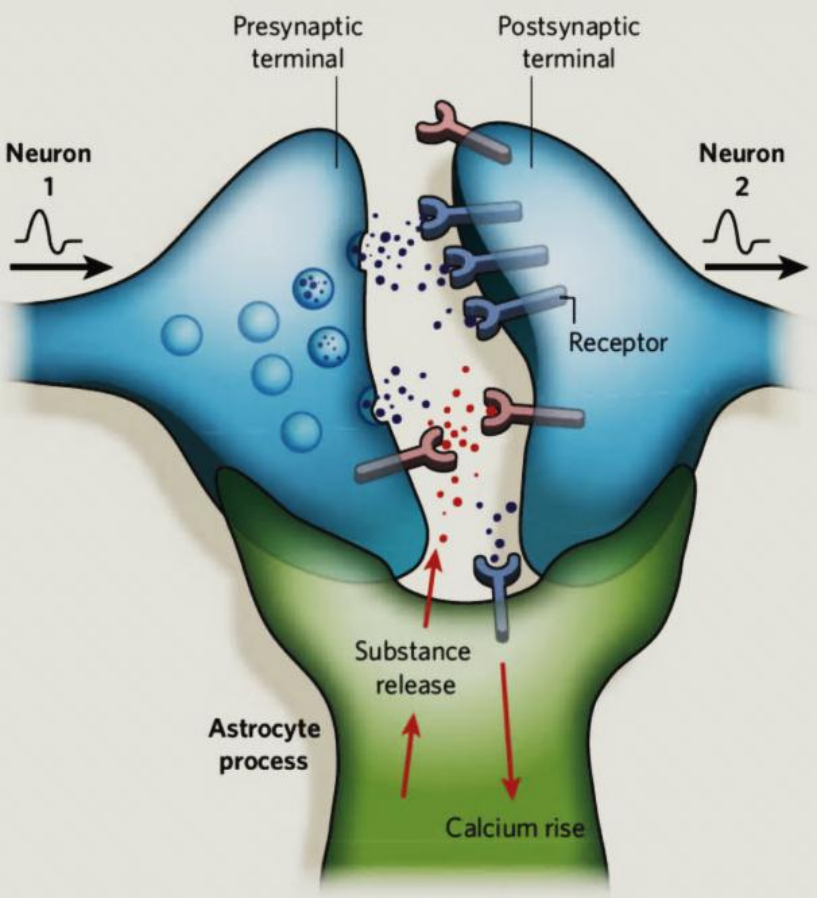

Figure 6. Tripartite synapse. Astrocytes can sense synaptic transmission by expressing receptors for neurotransmitters. Activation of these receptors by appropriate substance, such as glutamate, can lead to astroglial signaling that enhances or inhibits neuronal activity (Allen and Barres, 2009)

The principle of tripartite synapse was based on observations, that neuronal activity triggers Ca^{2+}-dependent release of gliotransmitters from astrocytes, placing them into position of active participants in fast synaptic information transfer (Araque et al., 1999). Although Ca^{2+}-dependent release of gliotransmitters from astrocytes was clearly demonstrated in vitro, importance of its role in vivo remains elusive due to lack of direct evidence supporting this theory (Hamilton and Attwell, 2010). Recently Sun and colleagues showed that expression of metabotropic glutamate receptors (mGluR) 5, which were believed to mediate glutamate-induced Ca^{2+}increase accompanied with gliotransmitter release from astrocytes, is developmentally regulated and is not detectable after postnatal week 3 in mouse astrocytes. This leads to impairment of Ca^{2+}-induced gliotransmission in adult mice (Sun et al., 2013). It seems that the main role of astrocytes in tripartite synapses is to shield synapses from interference of extrasynaptic signals and thus to keep synaptic transmission spatially and temporally precise, rather than to contribute to fast synaptic transmission (Hamilton and Attwell, 2010; Nedergaard and Verkhratsky, 2012). Along with Ca^{2+}-dependent release of gliotransmitters from astrocytes, which is still matter of debate, there are other pathways allowing transmitters to leave astrocytes. However, these mechanisms, like reversal of glutamate transporters EAAT1 and EAAT2 or activation of volume-regulated anion channels (VRACs), are usually initiated under pathological conditions (see the chapter 5.2).

3.2 Neurotransmitter receptors in astrocytes

Apart from release of gliotransmitters, astrocytes possess another mechanism to sense and modulate synaptic activity. They are equipped with a wide range of receptors for neurotransmitters (Verkhratsky and Steinhäuser, 2000; Verkhratsky et al., 2012). It is generally accepted that activation of astroglial metabotropic receptors triggers Ca^{2+} transients and promotes astroglial Ca^{2+} waves through activation of $InsP_3$ receptors on endoplasmic reticulum.

Moreover, astroglial metabotropic receptors represent a tool for regulation of local blood-flow through inducing release of vasoactive molecules from astrocytes (Verkhratsky et al., 2012). Apart from metabotropic receptors, astrocytes also express variety of inotropic receptors activated by glutamate, ATP, γ-aminobutyric acid (GABA) or glycine (**Table 1**) (Lalo et al., 2011c; Parpura and Verkhratsky, 2013).

Table 1. Astroglial ionotropic receptors, their ligands and function.

ligand	type	function
glutamate	AMPA	Na^+ influx, K^+ eflux - cell depolarization
	NMDA	Na^+ and Ca^{2+} influx, K^+ eflux - cell depolarization
ATP	$P_2X_{1/5}$	Na^+ and Ca^{2+} influx, K^+ eflux - cell depolarization
	P_2X_7	Channel pore permeable for molecules up to 900 Da
GABA	$GABA_A$	Cl^- eflux and cell depolarization
glycine	---	Cl^- eflux and cell depolarization

AMPA, α-amino-3-hydroxy-5-methyl-4-isoxazolepropionic acid; NMDA, N-methyl-D-aspartate; P_2X_7, P_2X purinoreceptor 7; $P_2X_{1/5}$, P_2X purinoreceptor 1/5; $GABA_A$, γ-aminobutyric acid receptor A; Da, Dalton

3.3 NMDA RECEPTORS

When glutamate was found to be the major excitatory neurotransmitter in mammalian CNS, it was believed that it can mediate only interneuronal communication. However, in 1984 Bowmam and Kimelberg showed that glutamate depolarizes also astrocytes (Bowman and Kimelberg, 1984). From this finding a growing body of evidence supports the idea of glutamate-mediating neuronal-astroglial communication. Three types of ionotropic glutamate receptors (iGluRs) are recognized, (i) α-amino-3-hydroxy-5-methyl-isoxazole propionate (AMPA) receptors, functionally characterized in astrocytes of many brain regions (Seifert and Steinhäuser, 2001; Lalo et al., 2006; Palygin et al., 2010), (ii) kainate receptors, which were detected in astrocytes at transcript and protein levels, but not functional level (Seifert and Steinhäuser, 2001), and (iii) N-methyl-D-aspartate (NMDA) receptors.

Generally, NMDA receptors are essential for normal brain function. They are responsible for excitatory neurotransmission and play critical role in modulation of synaptic strength that is believed to underlie memory, development and also some neurological diseases. Dysfunction of NMDA receptors causes many neuropathologies and thus they represent a great target for new therapies directed to treatment of neurological disorders such as Alzheimer´s disease or stroke. In general, NMDA receptors form heterotetrameric complexes assembled from seven distinct subunits (GluN1, GluN2A-D and GluN3A-B). It is believed that GluN1 is essential for proper receptor function, while GluN2 and GluN3 alone are not sufficient to form functional receptor (**Fig. 7**)(Paoletti and Neyton, 2007; Sobolevsky et al., 2009). NMDA receptors exhibit several specific features that allow them to integrate neuronal circuitry and modulate synaptic plasticity. These features include exceptionally high Ca^{2+} permeability and voltage-dependent sensitivity to Mg^{2+} block, which prevents NMDA receptor function at resting membrane potential.

Therefore, NMDA receptor-mediated Ca^{2+} fluxes occur only when Mg^{2+} block is removed by sufficiently strong depolarization of postsynaptic density relevant for synaptic plasticity (Malenka and Nicoll, 1999).

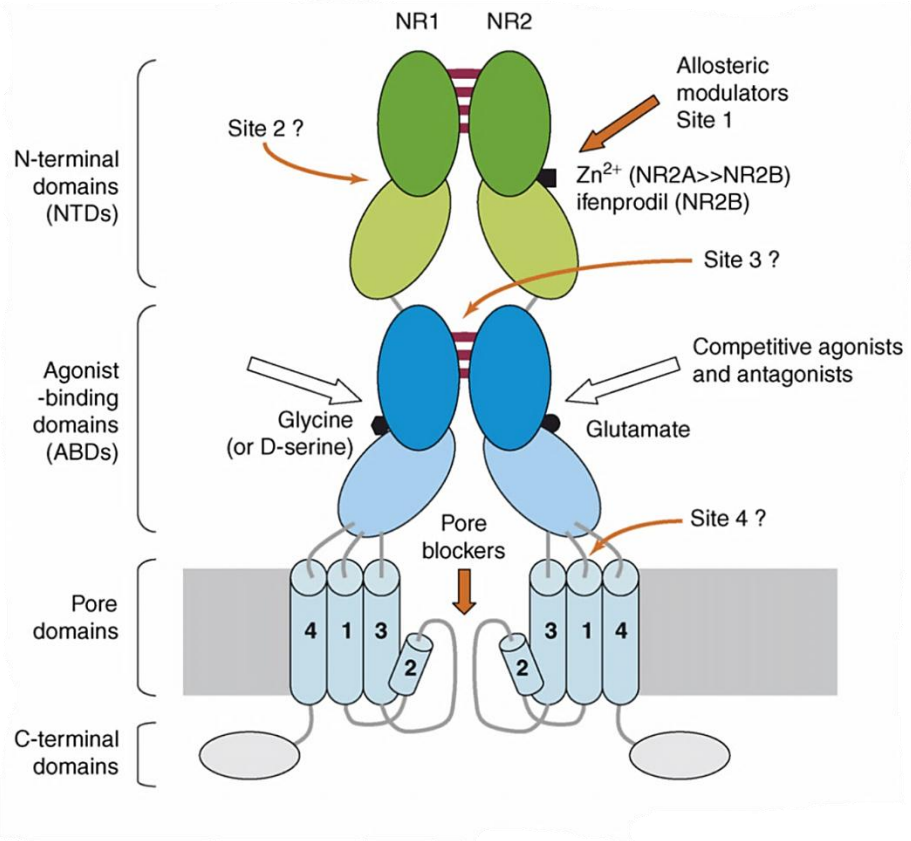

Figure 7. Scheme of NMDA receptor. NMDA receptors assemble as tetramers, that most often associate two GluN1 and two GluN2 subunits in a "dimer of dimers" architecture. The extracellular part of each subunit consists of N-terminal domain (NTD) and agonist-binding domain (ABD). ABD of GluN2 subunit binds glutamate, whereas ABD of GluN1 subunit binds co-agonists glycine/D-serine and only coincident binding of both can fully activate the receptor. White arrows indicate binding site of agonists/competitive agonists binding. Thick orange arrows show the site of non-competitive antagonist binding, such as Zn^{2+} or ifenprodil-like compounds. Channel pore is the site of action of channel blockers such as Mg^{2+}, MK-801 or memantine. The thin orange arrows indicate sites for putative modulatory sites, which can bind either positive or negative allosteric modulators (Paoletti and Neyton, 2007). NR, subunit of NMDA receptors; NTD, N-terminal domain; ABD, agonist-binding domain.

3.4 NMDA RECEPTORS IN ASTROCYTES

NMDA receptors were for a long time considered to be exclusively neuronal, because their activation requires membrane depolarization, which is in astroglial cells unlikely as they maintain resting membrane potential at relatively negative value (-80 mV) and it is difficult to depolarize them. However, during the last two decades, NMDA receptor subunits in astrocytes from different brain regions, including cerebral cortex, hippocampus or cerebellum, were detected by immunohistochemistry (Conti et al., 1996, 1999; Lee et al., 2010), reverse transcription-polymerase chain reaction (RT-PCR)(Akazawa et al., 1994; Schipke et al., 2001; Lee et al., 2010; Zhou et al., 2010) and in situ hybridization (Cahoy et al., 2008). Moreover, NMDA evoked currents and Ca^{2+} responses were recorded from astrocytes as well (Latour et al., 2001; Schipke et al., 2001; Zhang et al., 2003). Probably most intriguing results challenging the role of NMDA receptors in astrocytes were published recently (Lalo et al., 2006, 2011b; Palygin et al., 2010, 2011). The authors showed that after stimulation of nearby neurons, astrocytes generate excitatory currents sensitive to NMDA receptor antogonists, such as Dizocilpine (MK-801), D-2-amino-5-phosphonopentanoic acid (D-AP5) or (2R*,3S*)-1-(Phenanthrenyl-3-carbonyl)piperazine-2,3-dicarboxylic acid (UBP-141), but not ifenprodil. Furthermore they proved presence of NMDA receptors in acutely isolated astrocytes by measuring NMDA evoked inward currents and intracellular Ca^{2+} elevations, which were both sensitive to MK-801, D-AP5 and UBP-141.

Astroglial NMDA receptors differ from neuronal in one important feature. They show almost no sensitivity to Mg^{2+} block (Lalo et al., 2006). This is crucial for the function of NMDA receptors at astroglial negative membrane potential. The molecular basis of astroglial NMDA receptor insensitivity to Mg^{2+} block dwells probably in the presence of GluN3 subunit, which was shown to reduce Mg^{2+} sensitivity when incorporated into NMDA receptor. Furthermore, presence of GluN3 subunit significantly reduces Ca^{2+}permeability of NMDA receptors

(Henson et al., 2010). Astroglial NMDA receptors can be antagonized by UBP-141, which indicates presence of GluN2D subunit, while their insensitivity to ifenprodil excludes the presence of GluN2B subunit. Since presence of GluN2A transcript and protein was barely detected, the most probable composition of astroglial NMDA receptors is the tri-heteromeric assembly including GluN1, GluN2C/D and GluN3 subunit.

3.5 NMDA RECEPTORS IN ASTROGLIAL SIGNALING

Although direct electrophysiological experiments demonstrate that astrocytes are able to generate excitatory currents evoked by activation of astroglial NMDA receptors, the physiological role of these currents remains unclear. Since astrocytes are electrically non-excitable and even cannot be substantially depolarized due to large K^+ conductivity, the most probable function of astroglial NMDA receptors is to generate local increases of Na^+ and Ca^{2+} concentration in perisynaptic processes, which allows astrocytes to control and support synaptic transmission in many ways (**Fig. 8**).

Increase of intracellular concentration of Na^+ contributes to local Ca^{2+} signaling by controlling the function of Na^+/Ca^{2+}exchanger (NCX). High Na^+ concentration can reverse NCX and induce additional Ca^{2+} influx (Kirischuk et al., 1997). Na^+ is also coupled with $H^+/OH^-/HCO_3^-$ transporter and affects thus cytoplasmic pH values. Decrease in transmembrane Na^+ gradient after activation of NMDA receptors leads to reduction of glutamate uptake efficacy, which in turn prolongs excitatory postsynaptic potential, and therefore facilitates synaptic transmission. On the other hand, Na^+ influx stimulates activity of Na^+/K^+-ATPase, which leads to lowering of extracellular K^+ concentration resulting in hyperpolarization of neurons and therefore in suppression of neuronal excitability. Maybe the most important process associated with increase of cytoplasmic Na^+ concentration is stimulation of lactate production by aerobic

glycolysis. Lactate is then released from astrocytes and taken up by neurons where it is used as an energy substrate for active synapses (Lalo et al., 2011b).

In summary, the main role of astrocytes is to shield synapses, modulate synaptic strength by controlling extracellular concentration of K^+ and glutamate, and at the same time, support active neurons with energy substrate.

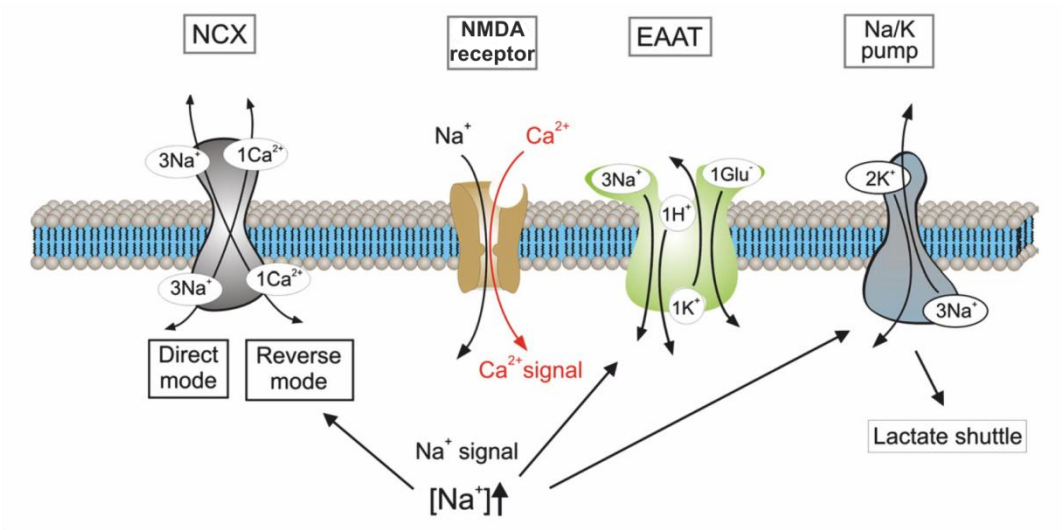

Figure 8. Processes related with NMDA receptors signaling in astrocytes. Activation of NMDA receptors triggers rise in intracellular concentration of Na^+ and Ca^{2+}, which affect function of many metabolic and homeostatic mechanisms including NCX, Na^+/K^+-ATPase or glutamate transporter EAAT (Lalo et al., 2011b). NCX, Na^+/Ca^{2+}exchanger; EAAT, excitatory amino acid transporter; $[Na^+]$, sodium concentration

4 CEREBRAL ISCHEMIA

Ischemia is defined as reduction of blood flow sufficient to alter normal cellular function. Brain tissue and especially neurons are very sensitive to ischemia due to their high energetic metabolism. Therefore, even brief ischemic period can trigger cascade of events, which can ultimately result in neuronal death. Depending on the cause of the injury, we distinguish two types of ischemic brain injury: global and focal cerebral ischemia.

4.1 GLOBAL VS. FOCAL CEREBRAL ISCHEMIA

Global cerebral ischemia develops after temporary interruption of cerebral blood flow caused by cardiac arrest with resuscitation or after near-drowning. Interruption of blood supply leads to loss of consciousness within approximately 10 seconds and a few minutes of global ischemia result in irreversible cellular damage. Depending on duration of global ischemia, neurons show delayed death (the susceptibility of neurons differs among different brain regions), whereas glial cells are spared and even become activated and proliferate to form glial scar (Pekny and Nilsson, 2005; Sun et al., 2006). Although neurons and glial cells are able to survive under ischemic conditions for a limited time period, global ischemia lasting longer than 10 minutes is lethal for men (Nedergaard and Dirnagl, 2005).

In contrast to above described ischemic injury focal cerebral ischemia is caused by transient or permanent blood flow reduction in the territory of brain artery due to embolic or thrombotic vessel occlusion. In the territory of occluded vessel necrotic death of all brain cell types occurs. This region, termed infarct core, is surrounded by ischemic penumbra, which is the ischemic border zone, where blood supply is partly maintained. Cells in this region remain metabolically active, but electrically silent (Astrup et al., 1981). The fate of penumbra depends on many factors, such as vascular territory or severity of blood flow reduction, but in general, cells in proximal part of penumbra tend to undergo apoptosis and

are included into the infarct core, whereas cells in distal part of penumbra are spared from cell death and exhibit only scattered injury (**Fig. 9**)(Nedergaard and Dirnagl, 2005).

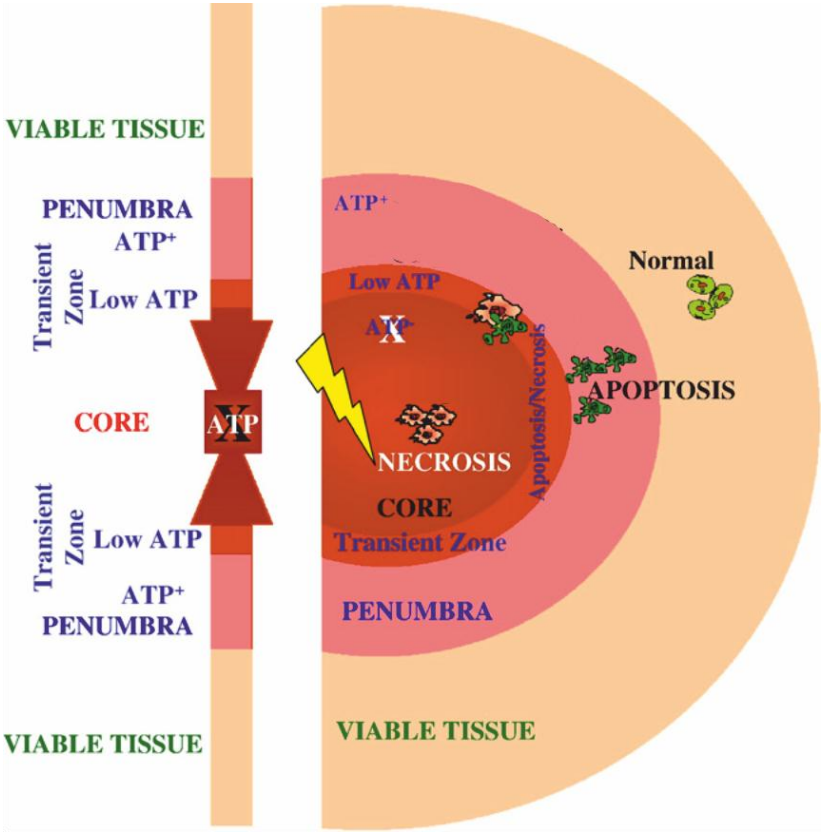

Figure 9.A Brain damage during cerebral ischemia: In infarct core all cell types undergo necrosis. In the penumbra the cells show delayed death (apoptosis) due to availability of ATP. The transient zone between core and penumbra is likely to merge to the ischemic core, if blood flow is not rapidly restored. The penumbra is surrounded by viable tissue (Mehta et al., 2007). ATP, adenosine triphosphate.

4.2 Pathophysiology of cerebral ischemia

The primary consequence of attenuated blood flow is loss of energy substrates, namely oxygen and glucose, which are crucial for production of ATP through glycolysis and oxidative phosphorylation. Since glucose can be temporarily substituted by alternative substrates like glycogen, lactate or fatty acids, oxygen is irreplaceable driver of mitochondrial respiration and thus the

main source of cellular ATP. The absence of oxygen leads to gradual depletion of cellular ATP due to its ongoing consumption (Silver et al., 1997). Since oxygen acts as final acceptor of electrons originating in respiratory chain, its absence allows electron leakage that results in generation of reactive oxygen species (ROS) (Abramov et al., 2007). Furthermore, when respiration is attenuated, persistent glycolysis leads to accumulation of protons and lactate causing rapid intracellular acidification (**Fig. 10**)(Silver et al., 1997). Although intracellular acidification and generation of ROS are stressful for most cells, it is primarily loss of ATP and consequent failure of ATP-dependent processes, which makes brain so sensitive to ischemic damage.

Indeed, inhibition of Na^+/K^+-ATPase and other ATP-dependent ionic pumps during ischemia, causes, after several minutes, loss of ionic gradients and membrane depolarization in neurons as well as in glial cells (**Fig. 10**)(Silver et al., 1997).

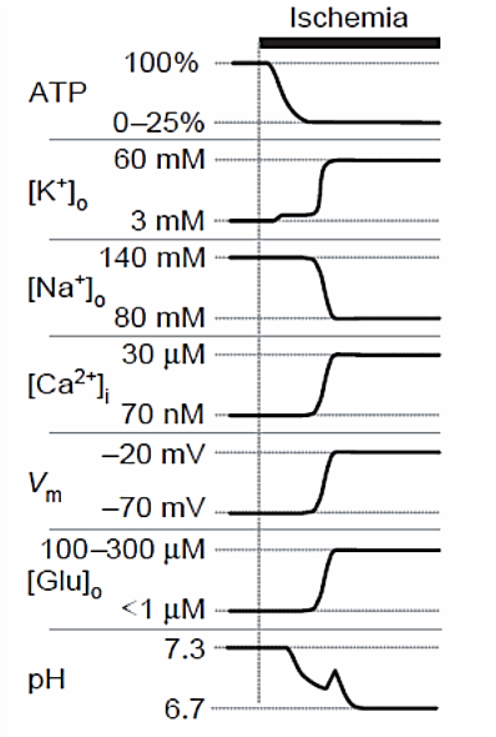

Figure 10. Events in global cerebral ischemia or in the core of focal cerebral ischemia. Attenuation of ATP production leads to dissipation of ionic gradients across the membrane. The disregulation of ionic homeostasis causes membrane depolarization and subsequent release of glutamate into extracellular space. Ischemia also leads to acidification (Rossi et al., 2007). $[K^+]_o$, extracellular potassium concentration; $[Na^+]_o$, extracellular sodium concentration; $[Ca^{2+}]_I$, intracellular calcium concentration; V_m, membrane potential; $[Glu]_o$, extracellular glutamate concentration.

The dissipation of ionic gradients is associated with two cross-linked processes: (i) large release of glutamate and other neurotransmitters into the extracellular space (**Fig. 10**)(Phillis et al., 1996) and (ii) swelling of neurons and glial cells (Silver et al., 1997; Kimelberg, 2005). Glutamate release triggers positive feedback loop by activating glutamate receptors of AMPA and NMDA type, which results in further depolarization and consumption of ATP, processes that both promote release of glutamate and cell swelling. In addition, astrocyte swelling contributes to glutamate release via activation of VRACs (Feustel et al., 2004). All these events eventually result in large increase of intracellular Ca^{2+} concentration (**Fig. 10**), which initiate the death of neurons and potentially also glial cells by process known as excitotoxicity (Won et al., 2002; Onténiente et al., 2003). Glutamate-induced excitotoxicity is a complex process, which involves activation of Ca^{2+}-dependent protein effectors like calpains, cytosolic phospholipases and endonucleases, which together with ROS, cause damage of cellular components and lead to cell death by necrosis or apoptosis (Won et al., 2002; Onténiente et al., 2003). In the moderately hypo-perfused penumbra the loss of ATP is not too severe to cause fatal ionic disruption, which occurs in the core, but it rather triggers repeated transient ischemic depolarizations (TIDs) (**Fig. 11**). Such TIDs can either develop into terminal depolarization and death of cells, or it can fade away with no cellular loss (Higuchi et al., 2002). In contrast to rapid TIDs, extracellular concentration of glutamate in penumbra increases gradually during first hour of ischemia and then declines to nearly preischemic values within 2-3 hours (Feustel et al., 2004).

Processes described above can affect neurons as well as glial cells, however neurons have higher density of ionotropic glutamate receptors and worse ability to keep ionic gradients and ATP levels, which makes them far more susceptible to ischemic damage than glial cells (Silver et al., 1997; Xie et al., 2008). These cell-specific features underlie selective destruction of neurons under ischemic conditions and place glial cells into the role of potential

protectors of their neighboring neurons, similarly to their supportive function in the healthy brain.

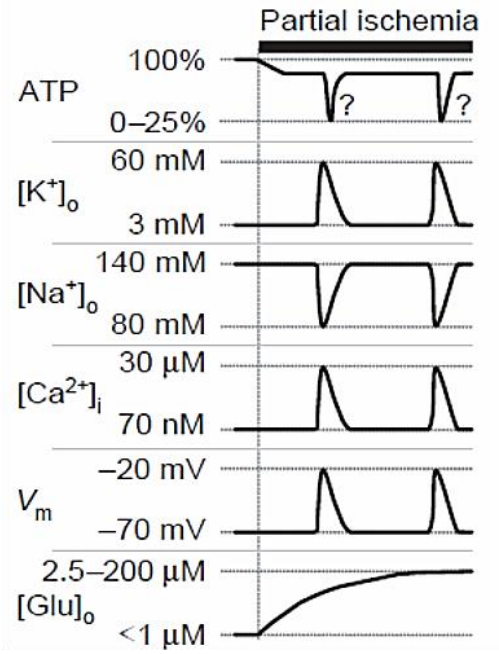

Figure 11. Events in penumbra of focal cerebral ischemia. In the penumbra the initial decline of ATP is less severe than in the infarct core, however itl triggers transient ischemic depolarizations with associated ion fluxes, while extracellular glutamate concentrations rise gradually (Rossi et al., 2007). $[K^+]_o$, extracellular potassium concentration; $[Na^+]_o$, extracellular sodium concentration; $[Ca^{2+}]_I$, intracellular calcium concentration; V_m, membrane potential; $[Glu]_o$, extracellular glutamate concentration.

5 Astrocytes in cerebral ischemia

As was mentioned above, astrocytes are far less susceptible to ischemic damage than neurons. In the case of focal ischemia, astrocytes are able to survive in regions where neurons died and together with NG2-glia and microglia form the border of infarct core. In this border zone, astrocytes are activated and proliferate to form glial scar, which physically separates damaged part of CNS from the healthy tissue (Pekny and Nilsson, 2005). Under ischemic conditions, astrocytes exhibit complex sequences of pathophysiological events, which can have both, positive or negative impact on tissue survival.

5.1 Astroglial glycogen

The primary cause of ischemic damage is deficit of ATP in brain cells. Under ischemic conditions, astrocytes are able to keep ATP at sufficient level for longer time than neurons, because they have lower demand of energy used for maintaining of ionic gradients due to lower density of ion channels when compared to neurons. Moreover, they store most of the brain glycogen, which can be used as alternative energy substrate for astrocytes as well as for neurons. However, the role of astroglial glycogen under ischemic conditions is not clear. The primary benefit of glycogen lies in production of lactate, which can be oxidized to produce ATP (Pellerin et al., 2007). In the absence of O_2, this benefit is changed to harmful lactic acidosis, which can even increase cellular damage caused by ischemia (Li et al., 1995). However, in regions where less severe ischemia occurs and ability to oxidize lactate is at least partially maintained, glycogen can contribute to preserving energy demands of astrocytes and neurons.

5.2 Swelling of astrocytes

Redistribution of ions during ischemic period is accompanied with water fluxes and consequent astrocyte swelling. There were described many

mechanisms that contribute to astrocyte swelling during ischemia. Inhibition of Na^+/K^+-ATPase leads to accumulation of Na^+ (together with Cl^-) in the astrocytes, which results in cell swelling. Moreover, an increase in extracellular K^+, which is a result of excessive neuronal activity, stimulates inwardly directed K^+ and Cl^- fluxes further promoting astrocyte swelling. Also intracellular acidification caused by accumulation of H^+ and lactate inside the cells contributes to astrocyte swelling by activation of Na^+/H^+ and Cl^-/HCO_3^- exchangers. Other mechanisms like excessive activation of glutamate transporters, astroglial AMPA and NMDA receptors or $Na^+/K^+/2Cl^-$ co-transporter, which can contribute to swelling of astrocytes, are schematically depicted in **Figure 12**. All described mechanisms lead to increase of intracellular osmolality, which drives water into astrocytes through AQP4. As astrocytes occupy 20-30 % of brain volume, their swelling markedly contributes to ischemia induced brain edema, which further worsens the ability of cells to survive (Kimelberg, 2005).

5.3 Astroglial glutamate handling

One of the major causes of neuronal death during ischemia is glutamate excitotoxicity. As under physiological conditions, astrocytes remove excessive glutamate from extracellular space also during ischemia. It was shown that during early phases of global ischemia astrocytic glutamate transporters take up glutamate and thus protecting neurons from excitotoxic damage (Ottersen et al., 1996; Hamann et al., 2002; Mitani and Tanaka, 2003). In global ischemia lasting longer than 10-15 minutes or in the core of focal ischemia glutamate starts to accumulate in cytoplasm of astrocytes, because the conversion of glutamate to glutamine is not efficient. Consequently, glutamate can be released by astrocytes via reversal of glutamate transporters (Ottersen et al., 1996). Astrocytes in penumbral region are able to keep their ATP levels for longer time, and therefore conversion of glutamate to glutamine as well as maintaining the membrane potential is preserved.

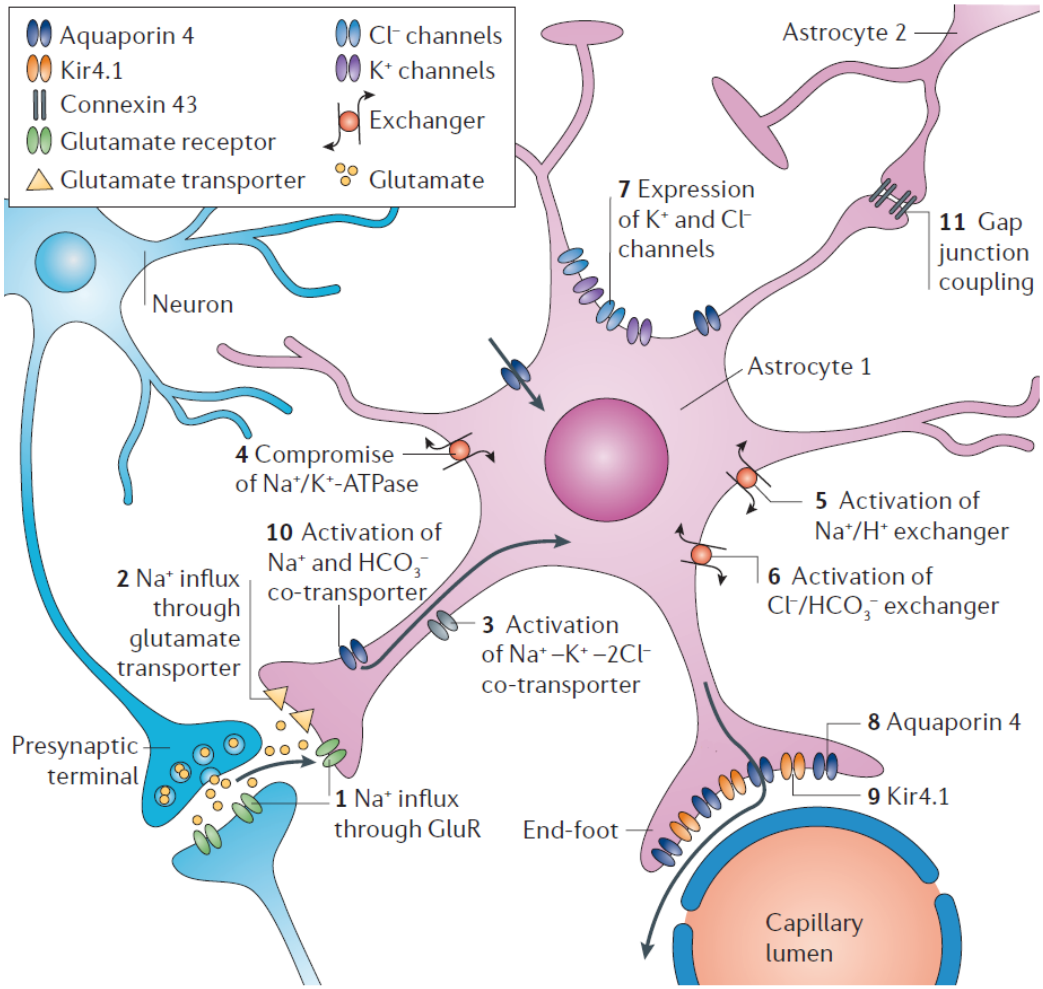

Figure 12. Swelling related mechanisms. Neuronal swelling seems to result from Na^+ influx through AMPA, NMDA and kainate receptors (**1**), Cl^- influx and water entry. On the other hand, astroglial swelling is much more complex process, which comprises many mechanisms. Na^+ influx can be driven by glutamate transporters (**2**) and receptors (**1**), high extracellular concentrations of K^+ can cause swelling through Na^+/ K^+/ $2Cl^-$ co-transporter (**3**). Astroglial swelling involves mechanisms observed also in other cell types, inluding compromised function of Na^+/K^+-ATPase (**4**), activation of Na^+/H^+ exchanger (**5**), Cl^-/HCO_3^- exchangers (**6**) or Na^+/HCO_3^- cotransporter (**10**). Various K^+ and Cl^- channels are expressed during astrocytic swelling of (**7**). AQP4 (**8**) are exclusively astroglial water permeable channels, which are together with Kir4.1 (**9**) the main contributors to water and K^+ fluxes and spatial buffering, which is also dependent on astroglial gap-junction (**11**) network (Seifert et al., 2006). Kir4.1, inwardly rectifying K^+ channels 4.1; GluR, glutamate receptors.

Both of these processes help astrocytes to take up glutamate from extracellular space, which allows them to protect neurons for longer time period of ischemia (Rao et al., 2001; Feustel et al., 2004). The beneficial role of glutamate uptake is partially compensated by swelling-induced release of glutamate and other amino acids through astroglial VRACs in process known as regulatory volume decrease (Kimelberg, 2005). It is believed that release of glutamate mediated by VRACs strongly contributes to ischemic damage, because VRACs antagonists reduce glutamate release from astrocytes in ischemic core as well as in penumbra and provide thus significant neuroprotection (Seki et al., 1999; Feustel et al., 2004; Kimelberg, 2005).

5.4 Role of astroglial gap junctions and hemichannels

Gap junctional network provides direct coupling between astrocytes forming astroglial syncytium. Apart from gap junctions astrocytes also express hemichannels, which allow small molecules to pass between cytoplasm and extracellular space. These hemichannels are open during ischemia and contribute to damage of cells by allowing influx of Na^+ and Ca^{2+} into the cell. There is also evidence suggesting that these channels are able to release glutamate to promote additional cell damage (Ye et al., 2003). Although astroglial gap junctional coupling is reduced in ischemia, it still provides inter-glial signaling. Precise role of gap junctions under ischemic conditions remains unclear, however it is generally accepted that in the case of focal ischemia gap junctions allow toxic molecules to pass from dying astrocytes in the infarct core to the viable astrocytes in the penumbra. And conversely, gap junctions allow survival promoting molecules from penumbral astrocytes to diffuse to the dying cells. Whether this coupling eventually leads to protection of dying cells or to damage of viable cells depends on many factors such as degree of conductance, type of channels and ratio between viable and dying cells (**Fig. 13**). Taken together, it is difficult to evaluate the overall contribution of coupling between

core and penumbral astrocytes, because of inability to selectively block gap junctions without blocking hemichannels and also because of large number of toxic and survival-promoting molecules, which should be considered (Contreras et al., 2004)

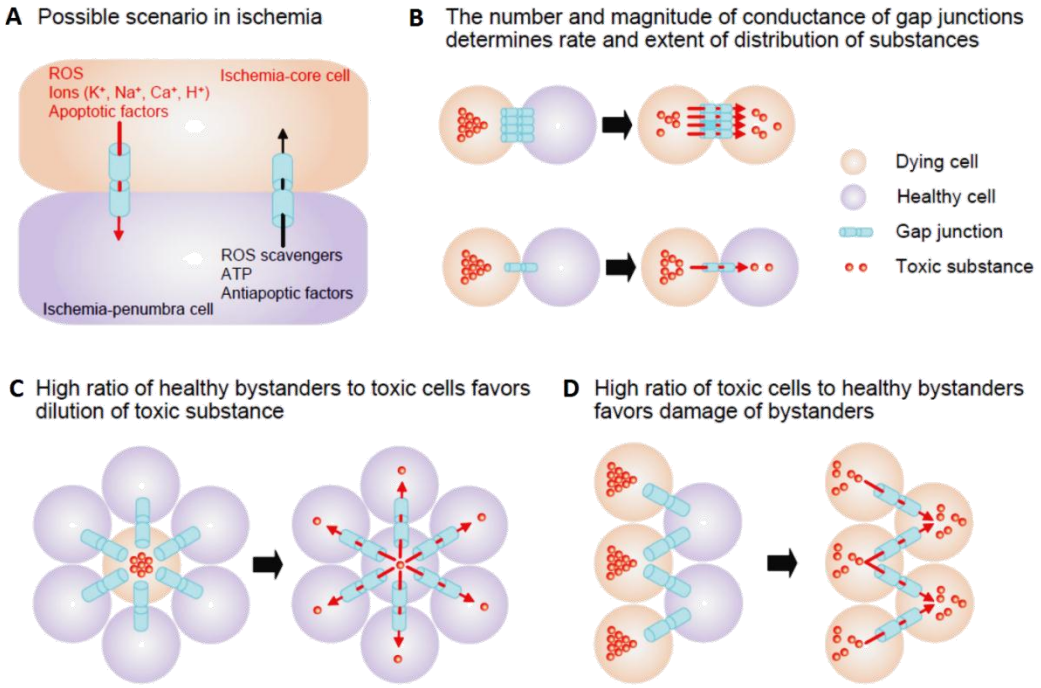

Figure 13. Scheme of possible interaction between viable and ischemia-damaged astrocytes though gap-junctions. A) toxic molecules pass from dying astrocytes in the infarct core to the viable astrocytes in the penumbra and conversely, survival promoting molecules from penumbral astrocytes diffuse to the dying cells. **B)** The rate of conductivity and the number of gap junction together with ratio between viable and dying cells (**C,D**) determines whether the coupling provide protection for dying cells or destruction for viable cells (Rossi et al., 2007). ROS, reactive oxygen species

5.5 Astroglial NMDA receptors

Only a few studies examined astroglial NMDA receptors in context of cerebral ischemia. GluN1, GluN2A and GluN2B were detected by immunohistochemistry in astrocytes of the rat CA1 region of the hippocampus after transient global ischemia, but not in the healthy animals and in cultured hippocampal astrocytes after 5 minutes of anoxia (Gottlieb and Matute, 1997; Krebs et al., 2003). Furthermore NMDA-evoked Ca^{2+} rises were recorded in cultured hippocampal astrocytes after 5 minutes of anoxia as well as in astrocytes isolated acutely from the ischemic hippocampus (Krebs et al., 2003). Recently Zhou and co-workers showed by RT-PCR that expression of mRNA coding GluN1, GluN2A and GLUN2B in cultured mouse hippocampal astrocytes is developmentally and ischemia-regulated process. The subunits GluN1 and GluN2B are significantly up-regulated after 2 hours of oxygen glucose deprivation (OGD), while GluN2A is after 6 hours of OGD down-regulated (Zhou et al., 2010).

The expression of NMDA receptors in post-ischemic astrocytes seems to be controlled by the processes related to accompanying death of neurons, such as an increase in extracellular glutamate, the cellular debris generated by neuronal damage or substances produced by activated microglia (Gottlieb and Matute, 1997). However, the precise mechanism that triggers expression of NMDA receptors as well as their role, either protective or detrimental, in ischemic astrocytes remains largely unknown.

6 AIMS OF THE THESIS

- To identify the changes in the expression profile of astrocytes following ischemic injury with main focuse on NMDA receptor subunits

- To elucidate the changes in the expression of NMDA receptor subunits on the protein level in reactive astrocytes following ischemia

- To characterize electrophysiological properties of cortical astrocytes *in situ* as well as *in vitro*

- To study the NMDA-specific responses in cortical astrocytes after ischemic injury using intracellular Ca^{2+} imaging

7 MATERIALS AND METHODS

7.1 TRANSGENIC MICE

Experiments were performed on transgenic mice, in which astrocytes are labeled by the enhanced green fluorescent protein (EGFP) under control of the human glial fibrillary acidic protein (GFAP) promotor (Nolte et al., 2001). For all experiments were used 40-60 days old mice (male).

7.2 SOLUTIONS

Composition of all used solutions is listed in **Table 2**, pH values were estimated using pH-meter MiniLab IQ125 (IQ Scientific Instruments, Carlsbad, CA, USA). Osmolality was checked with a vapor-pressure osmometer (Vapro 5520, Wescor, South Logan, UT, USA), and when needed, adjusted with mannitol. All solutions were gassed with appropriate gas mixture. Isolation solution and bicarbonate-based artificial cerebrospinal fluid (aCSF) were gassed with 95% O_2/5% CO_2 while 4-(2-hydroxyethyl)-1-piperazineethanesulfonic acid (HEPES)-based aCSF was gassed with 100% O_2 in order to keep proper pH values and oxygen level. All chemicals were purchased from Sigma-Aldrich, St. Louis, MO, USA

7.3 INDUCTION OF DISTAL MIDDLE CEREBRAL ARTERY OCCLUSION IN ADULT MICE

Prior to middle cerebral artery occlusion (MCAo) induction mice were anaesthetized with 1.5% Isoflurane and maintained in 1% Isoflurane using a vaporizer (Tec-3, Cyprane Ltd., Keighley, UK). A skin incision between the orbit and the external auditory meatus was made. A 1-2 mm hole was drilled through the frontal bone 1 mm rostral to the fusion of the zygoma and the squamosal bone and about 3.5 mm ventral to the dorsal surface of the brain. The middle cerebral artery (MCA) was exposed after the dura was opened and removed. The MCA was occluded by short coagulation with bipolar tweezers at a proximal

location, followed by transection of the vessel to ensure permanent disruption. The body temperature during the surgery was maintained at 37±1°C using a heating pad. To visualize the ischemic region, unfixed brain slices were stained with 2% 2,3,5-triphenyltetrazolium chloride (TTC) at 37°C for 20 minutes.

All procedures involving the use of animals were approved by the local ethical review committee and were in agreement with European Communities Council Directive (86/609/EEC).

7.4 Preparation of acute brain slices

The brain slices were prepared from control mice as well as from those after MCAo. The mice were deeply anaesthetized with pentobarbital (PTB) (100 mg/kg, i.p.) and complete thoracotomy was made to expose the heart. After right atrium was cut open mouse was perfused transcardially through left ventricle with syringe filled with 20 mL of cold (4-8°C) isolation solution and decapitated. The head was placed on silicon-coated Petri dish filled with cold (4-8°C) isolation solution. After cutting the skin with scissors, the skull was cut along the midline and skull bones were removed using dissecting tweezers. The cerebellum and olfactory bulb were removed with scalpel and the rest of the brain was glued to the specimen disc with its ventral part leaning at agar cube. The specimen disc was then placed in the tray of the vibration microtome (HM 650 V, Thermo Scientific Microm, Walldorf, GER) filled with cold isolation solution. The transversal 200 µm thick slices were cut with razor blade and the slices were held at room temperature in bicarbonate-based aCSF.

Table 2. Composition of extracellular and intracellular solutions used for brain isolation, Ca^{2+}-imaging and patch clamp.

	isolation solution	bicarbonate-based aCSF	HEPES-based aCSF	intracellular solution
		concentration [mM]		
NMDG	110	---	---	---
NaCl	---	122	135	12
KCl	2.5	3	2.7	120
$NaHCO_3$	24.5	28	---	---
HEPES	---	---	10	10
Na_2HPO_4	1.25	1.25	1	---
Glucose	20	10	10	---
$MgCl_2$	7	1.3	1	---
$CaCl_2$	0.5	1.5	2.5	---
OGB1	---	---	---	0.2
Mg-ATP	---	---	---	5
		pH		
pH	7.4	7.4	7.4	7.3
		mOsm/kg		
osmolality	305±5	305±5	305±5	285±5

All chemicals were purchased from (Sigma–Aldrich St. Louis, MO, USA). NMDG, N-methyl-D-glucamine; OGB1, Oregon Green BAPTA1; Mg-ATP, magnesium adenosine triphosphate.

7.5 Primary cortical astrocyte culture preparation

The primary astrocyte cultures were prepared from control mice as well as those after MCAo. Transcardial perfusion and the slices preparation were performed as described above, while thickness of slices was 400 µm. The cerebral cortex was mechanically disected out from the slices using scalpel and dissecting tweezers. In mice after MCAo, ischemic core with its surrounding (cca ½ of the injured hemisphere) was used. The isolated tissue was then cut into small

pieces by razor blade, transferred into falcon tube containing 1 mL of isolation solution containing 24 U/mL of papain and 0.24 mg/mL of cysteine and incubated for 45 minutes at 37°C under stirring. After incubation 1 mL of papain inhibitor was added and the mixture was gently triturated with 1mL pipet. After that 8 mL of cultivation medium (**Table 3**) was added and the mixture was centrifugated for 3 minutes at 2000 RPM. The supernatant was discarded and 6 mL of fresh cultivation media was added. The cells were resuspended, plated in 0.5 mL volumes onto coverslips and cultured in an incubator (100% humidity, 5% CO_2) at 37°C for 4-7 days.

Table 3. Composition of cultivation medium

	Dulbecco's modified Eagle's medium enriched with nutrient mixture F12 (DMEM/F12, Gibco, Life technologies, Carlsbad CA, USA)	
	concentration	
penicillin	100 U/mL	Gibco, Life technologies, Carlsbad, CA, USA
streptomycin	100 µg/mL	Gibco, Life technologies, Carlsbad, CA, USA
amphotericin B	25 µg/mL	Gibco, Life technologies, Carlsbad, CA, USA
fetal bovine serum (FBS)	15 %	Gibco, Life technologies, Carlsbad, CA, USA
glutamine	4 mM	Sigma-Aldrich, St. Louis, MO, USA

7.6 Single-cell gene expression profiling

Single-cell gene expression experiments were performed in collaboration with Laboratory of gene expression in Institute of Biotechnology AS CR, with intention to characterize gene expression profile of $EGFP^+$ cells. In this work only $EGFP^+$ cells that express genes for EAAT2 (Slc1a2) and glutamine synthase (Glul), both markers of astrocytes (Chaudhry et al., 1995; Wu et al., 2005) were considered and only 9 genes, from 47 characterized, were chosen for purpose of this work.

7.6.1 Preparation of cortical cell suspensions

Before the collection of single EGFP$^+$ cells via flow cytometry, the cortical tissue was dissociated using papain treatment. In the experiment, 50 days-old GFAP/EGFP mice (control - CTRL) and those 3, 7 and 14 days after MCAo (D3, D7, D14) were used. The animals were deeply anesthetized and perfused transcardially and cerebral cortex was isolated as described earlier (see the Methods, chapter 6.4). In mice after MCAo, ischemic core with its surrounding (cca ½ of the injured hemisphere) was used. The tissue was incubated with continuous shaking at 37°C for 90 minutes in 5 mL of a papain solution (20 U/mL) and 0.2 mL DNAase (both from Worthington, Lakewood, NJ, USA) prepared in isolation solution. After papain treatment the tissue was mechanically dissociated by gentle trituration using a 1 ml pipette. According to the manufacturer instructions dissociated cells were layered on the top of 5 mL of Ovomucoid inhibitor solution (Worthington, Lakewood, NJ, USA) and harvested by centrifugation (140 x g for 6 minutes). Cell aggregates were removed by filtering with a 30 nm cell strainer (Becton Dickinson, Franklin Lakes, NJ, USA), and the cells were kept on ice until sorting. This method routinely yielded cca 2 x 10^6 cells per mouse.

7.6.2 Collection of single EGFP+ cells by flow cytometry

The collection of single cells was performed using flow cytometer (Becton Dickinson, Franklin Lakes, NJ, USA), which was manually calibrated to deposit single cells in the center of each well of the 96-well plates (Applied biosystems, Life technologies, Carlsbad, CA, USA), which were placed on a pre-cooled rack. Only viable and EGFP$^+$ cells were collected. The viability of the cells was checked using Hoechst 33258 (Molecular Probes, Life Technologies, Carlsbad, CA, USA). Single cells were collected into 5 µL nuclease-free water with bovine serum albumin (1 mg/µL, Fermentas) and RNaseOut (20 U)(Invitrogen, Life

Technologies, Carlsbad, CA, USA). Collected cells in 96-well plates were immediately after sorting placed at -80°C.

7.6.3 Synthesis of cDNA

cDNA was synthesized using SuperScript III RT (Invitrogen, Life Technologies, Carlsbad, CA, USA). Lysed single cells were incubated at 70°C for 5 min in 5 µL water containing 0.5 µM dNTP (Promega, Madison, WI, USA), 1 µM oligo (dT15) (Invitrogen, Life Technologies, Carlsbad, CA, USA) and 1 µM random hexamers (Eastport, Prague, CZ). 50 mM Tris–HCl, 75 mM KCl, 3 mM $MgCl_2$, 5 mM dithiothreitol, 20 U RNaseOut and 100 U SuperScript III (Invitrogen, Life Technologies, Carlsbad, CA, USA) were added to a final volume of 10 µL. Reverse transcription was performed at 25°C for 5 min, then at 50°C for 60 min, followed by 55°C for 15 min and finally terminated by heating at 70°C for 15 min. 4 µL from each sample was diluted 4 times and used for pre-testing and another 5 µL of sample was used for cDNA pre-amplification.

7.6.4 Primer design and optimization of assays

All primers used in this work were designed using Beacon Designer (version 7.91, Premier Biosoft International). All primers were designed to span an intron to avoid amplification of genomic DNA. BLAST (Basic Local Alignment Search Tool) searches revealed no pseudogenes. All assays of single cells were optimized so as to not generate primer dimers before cycle 45, to have a PCR efficiency of at least 90%, and to amplify all known splice forms documented by the National Center for Biotechnology Information (NCBI). Calibration curves with purified PCR products (QIA quick PCR Purification Kit; Qiagen, Germany) were used to establish the linearity of the assays. The formation of the correct PCR products was confirmed by electrophoresis on 20 g/L agarose gels for all assays and by melting-curve analysis of all samples. Five individual cells per assay were tested, and no genomic DNA amplification was observed.

7.6.5 qPCR

All single cells were pre-tested for the expression of glutamate transporter (Eaat2), glutamine synthetase (Glul), both markers of astrocytes, chondroitin sulfate proteoglycan 4 (Cspg4) and platelet-derived growth factor α receptor (Pdgfαr), both markers of NG2 glia, to select samples for further gene expression profiling using assays for all 47 genes. A CFX384 (Biorad, Hercules, CA, USA) was used for all qPCR measurements. To each reaction (10 µL) containing iQ SYBR Green Supermix (BioRad, Hercules, CA, USA) and 400 nM of each primer (Eastport, Prague, CZ), we added 3 µL of diluted cDNA. The temperature profile was 95°C for 3 min followed by 50 cycles of amplification (95°C for 15 s, 60°C for 15 s and 72°C for 20 s). All samples were subjected to melting curve analysis. The same experimental setup was used to test pre-amplification.

7.6.6 Preamplification of cDNA and qPCR

To verify the pre-amplification protocol, the RNA from three animals was extracted and cDNA was prepared for the test of the protocol. Each reaction contained 25 µL of iQ Supermix (BioRad, Hercules, CA, USA), 5 µL of a mix of all primers (each in final concentration of 25 nM), 5 µL of non-diluted cDNA, and water added to a final volume of 50 µL. The temperature profile was 95°C for 3 min followed by 18 cycles of amplification (95°C for 20 s, 57°C for 4 min and 72°C for 20 s on a Biorad CFX96). The sample was diluted 5 times in water. The expression of all genes was measured in pre-amplified and non-pre-amplified samples. The average difference between pre-amplified and non-pre-amplified samples and the standard deviations of the differences were calculated and the same setup was used for the pre-amplification of single cells.

7.6.7 High throughput qPCR

The sample reaction mixture contained 2.4 µL of diluted pre-amplified cDNA, 0.25 µL of DNA Binding Dye Sample Loading Reagent (Fluidigm, San Francisco, CA, USA), 2.5 µL of SsoFast EvaGreen Supermix (BioRad, Hercules, CA, USA), and

0.01 µL of ROX (Invitrogen, Life Technologies, Carlsbad, CA, USA). The primer reaction mixture contained 2.5 µL Assay Loading Reagent (Fluidigm, San Francisco, CA, USA) and 2.5 µL of a mix of reverse and forward primers, corresponding to a final concentration of 4 µM. The chip was first primed with an oil solution in the NanoFlex™ 4-IFC Controller (Fluidigm, San Francisco, CA, USA) to fill the control wells of the dynamic array. The reaction mixture was loaded into each sample well, and primer reaction mixtures was loaded into each assay well of the 48x48 dynamic array. The dynamic array was then placed in the NanoFlex™ 4-IFC Controller for automatic loading and mixing. After 55 min the dynamic array was transformed to the BioMark qPCR platform (Fluidigm, San Francisco, CA, USA). The cycling program was 3 min at 95°C for activation, followed by 40 cycles of denaturation at 95°C for 5 s, annealing at 60°C for 15 s, and elongation at 72°C for 20 s. After PCR, melting curves were collected between 60°C and 95°C with 0.5°C increments.

7.6.8 Data processing

Data from qPCR were pre-processed before expression analysis using GenEx (MultiD, version 5.3). Quantification cycle (Cq) values registered from amplifications that generated melting curves with aberrant melting temperature (Tm) were removed, Cq values larger than 26 were replaced with 26, and Cq values with products giving rise to a double peak in melting curves (corresponding to a mixture of expected and aberrant PCR products) were replaced with 26. All missing data, for each gene separately, were then replaced with the highest Cq value increased by 2, effectively assigning a concentration of 25% of the lowest measured concentration to the off-scale values. The Cq data were, for each gene separately, converted into relative quantities expressed relative to the sample with the lowest expression (maximum Cq) and finally converted to a logarithmic scale with base 2. The data were not normalized to any reference genes because of the large variation of all transcript levels among

individual cells (Ståhlberg & Bengtsson 2010); with this pre-processing, the levels are expressed per cell.

7.7 Immunohistochemistry

The mice were deeply anaesthetized with PTB (100 mg/kg, i.p.) and perfused transcardially with 20 mL of saline followed by 20 mL of cooled 4% paraformaldehyde in 0.1 M phosphate buffer. Brains were dissected out, post-fixed for 18 hours and placed stepwise in solutions with gradually increasing sucrose concentrations (10%, 20%, 30%) for cryoprotection. Coronal, 30 µm thick slices were prepared using a microtome (HM550, Microm International, Germany). The slices were incubated with 5% Chemiblocker (Millipore, Billerica, MA, USA) and 0.2% Triton in phosphate buffer saline. This blocking solution was also used as the diluent for the antisera. The slices were incubated with the primary antibodies at 4-8°C overnight, and the secondary antibodies were applied for 2 hours. As primary antibodies we used anti-NMDAR1 (Abcam, Cambridge, UK, 1:500), anti-NMDAR2A (Abcam, 1:400), anti-NMDAR2B (Abcam, 1:400), anti-NMDAR2C (Alomone Labs, Jerusalem, Israel, 1:400), anti-NMDAR2D (Alomone Labs, 1:400), anti-NMDAR3A (Abcam, 1:400). As secondary antibody we used goat anti-rabbit immunoglobulin G conjugated with Alexa Fluor 594 (1:200, Molecular Probes, USA). The slices were mounted using Aqua Poly/Mount (Polysciences Inc., Eppelheim, GER). All chemicals were purchased from Sigma–Aldrich (St. Louis, MO, USA).

7.8 Confocal microscopy

To carry out immunohistochemical analysis, a Zeiss 510DUO LSM equipped with Arg/HeNe lasers and 40x oil objective was employed. Stacks of consecutive confocal images taken at intervals of 1 µm were acquired sequentially with the 2 lasers to avoid cross-talk between fluorescent labels. The background noise of each confocal image was reduced by averaging four image inputs. For each

image stack the gain and detector offset were adjusted to minimize saturated pixels, yet still permit the detection of weakly stained cell processes. Co-localization images and their maximum z projections were made using a Zeiss LSM Image Browser.

7.9 Electrophysiological experiments

Membrane currents were measured using patch-clamp technique in whole-cell configuration (Hamill et al., 1981). During the patch-clamp recordings, the microscope superfusion chamber was continually perfused with bicarbonate- or HEPES-based aCSF at a flow rate of 2.5 mL/min. Micropipettes were pulled from borosilicate capillaries with filament (Sutter Instruments Company, Novato, CA, USA) using horizontal P-97 Flaming/Brown Micropipette Puller (Sutter Instruments Company, Novato, CA, USA). The electrode had a resistance of 10-20 MΩ. Specimens were transferred into a recording chamber mounted on the stage of an upright microscope (Axioskop 2, FS plus, Carl Zeiss, Oberkochen, GER) equipped with a long-distance 10× (Achroplan 0.3 W, Ph 1, Zeiss, GER) and 40x (IR Achroplan 0.8 W, Zeiss, Germany) objectives, high-resolution digital camera (PCO Sensicam, Kelheim, GER) and electronic micromanipulators (Luigs& Neumann, Ratingen, GER). Current signals were amplified by means of EPC-10 amplifier (HEKA Elektronik, Lambrecht, GER) and lowpass-filtered at 3 kHz. Data acquisition, storage and analysis were performed with PatchMaster/FitMaster software (HEKA Elektronik, Lambrecht, GER). Current patterns were obtained in the voltage-clamp mode. The resting membrane potential (RMP) was measured by switching the amplifier to the current-clamp mode and the membrane resistance (R_m) was calculated from the current elicited by a 10-mV test pulse depolarizing the cell membrane from the holding potential of -70 mV to -60 mV for 50ms. The steady-state current value was taken 40 ms after the onset of the depolarizing pulse. Membrane capacitance (C_m) was determined automatically from the LockIn protocol by Patch Master. The basic current patterns were

obtained by clamping the cell membrane from the holding potential of -70 mV to values ranging from -160 mV to +40 mV for 50 ms at 10 mV intervals. The inwardly rectifying K^+ (K_{ir}) current component was determined by the subtraction of passive currents (the time- and voltage-independent current between -70 mV and -60 mV was multiplied by the relative potential jumps and subtracted from the corresponding current traces offline) from the current traces obtained by hyperpolarizing the cell membrane to -140 mV for 50 ms, 40 ms after onset of the depolarizing pulse. To isolate the voltage-gated delayed outwardly rectifying K^+ (K_{dr}) current component, a voltage step from -70 to -60 mV was used to subtract time- and voltage-independent currents. To activate the K_{dr} currents only, the cells were held at -50 mV, and the amplitude of the K_{dr} currents was measured at +40 mV, 40 ms after onset of the depolarizing pulse. The fast activating and inactivating outwardly rectifying K^+ (K_a) current component was isolated by subtracting the current traces clamped at -110 mV from those clamped at -50 mV, and its amplitude was measured at the peak value. Current densities were calculated by dividing the maximum current amplitudes by the corresponding C_m for each individual cell.

7.10 Fluorescent Ca^{2+}-imaging

During the intracellular Ca^{2+} measurements, the microscope superfusion chamber was continually perfused with HEPES-based aCSF at a flow rate of 2.5 mL/min. The NMDA receptors agonists (NMDA and glycine (Sigma–Aldrich St. Louis, MO, USA)) were applied through a capillary (i.d. 250 µm) located 0.5 mm from the selected cells. The capillary was connected to a Perfusion Pressure Kit pressurized application system (flow rate 600 µL/min) controlled by a ValveBank II controller (AutoMate Scientific, Inc. Berkeley, CA, USA). To verify that the response was not influenced by the application itself, HEPES-based aCSF was applied before and after application of NMDA receptors agonists with the same flow rate. Fluorescence was detected with a TILL Photonics Imaging System

installed on a Zeiss Axioskop 2 FS Plus microscope equipped with a long-distance 10× objective (Achroplan 0.3 W, Ph 1, Zeiss, GER) and long-distance 40× objective (IR Achroplan 0.8 W, Zeiss, GER). A digital camera (PCO Sensicam, Kelheim, GER) was controlled by TILLvisION software. The excitation light (488 nm) was generated by a Polychrome V (TILL Photonics GmbH, Gräfelfing, GER), filtered by a BP 450–490 excitation band-pass filter, reflected by a FT 510 beam splitter and the emitted light was filtered by a LP 515 long-pass filter (Filter Set 09, Zeiss, GER). Images were acquired at 0.83 Hz and were analyzed offline. Fluorescence intensity (F) was measured in the cell bodies. As response was considered changes in fluorescent intensity that was at least three times higher than noise level.

7.10.1 Recording in primary cortical astrocytic culture and in acute brain slices

Coverslips with 4-7-days old astrocytic culture were placed in the recording chamber superfused with extracellular solution at the flow rate 2,5 mL/min. The EGFP-labeled cells were found and coordinates of their location were registered. After that superfusion was stopped and coverslips were incubated for 45 minutes in 3 mL of HEPES-based aCSF containing 1 µM Oregon Green BAPTA-1-acetoxymethyl ester (OGB1-AM) (Sigma–Aldrich St. Louis, MO, USA) and 0.02% Pluronic F-127 (Invitrogen, Life Technologies, Carlsbad, CA, USA) at room temperature in the recording chamber. After incubation superfusion was turned on, excessive OGB1-AM was washed away, EGFP-labeled cells were re-located and 3-5 recordings were performed on one coverslip.

In situ recordings in control mice were performed in the cortical layer I/II 10-20 µm below the surface of the slices. In mice after MCAo, in situ recordings were performed in close surrounding of ischemic core. All procedures were performed exactly the same as in case of recording in primary cortical astrocytic

culture. In order to avoid neuronal activity tetrodotoxin (TTX) (Sigma-Aldrich, St. Louis, MO, USA) was used in several experiments experiment.

7.11 Data analysis

Data are presented as means ± S.E.M. (standard error of the mean) for n cells. One-way ANOVA test was used to determine significant differences between the experimental groups. Values of * $p<0.05$ were considered significant, ** $p<0.01$ very significant and *** $p<0.001$ extremely significant.

8 RESULTS

8.1 INDUCTION OF FOCAL CEREBRAL ISCHEMIA

To induce a focal cerebral ischemia, a highly reproducible model of mouse MCAo was employed (Kuraoka et al., 2009). Three days after MCAo the ischemic lesion developed in the dorsal brain and occupied approximately one-third of the cortex in the left hemisphere (**Fig. 14**). The necrotic tissue was surrounded by massive astrogliosis beginning 3 days after MCAo with a maximal intensity of GFAP staining 7 days after MCAo (**Fig. 14**). The size of the ischemic lesion and the intensity of GFAP staining gradually decreased starting on the seventh day of ischemia, and 14 days after MCAo the lesion comprised approximately 25% of its original size.

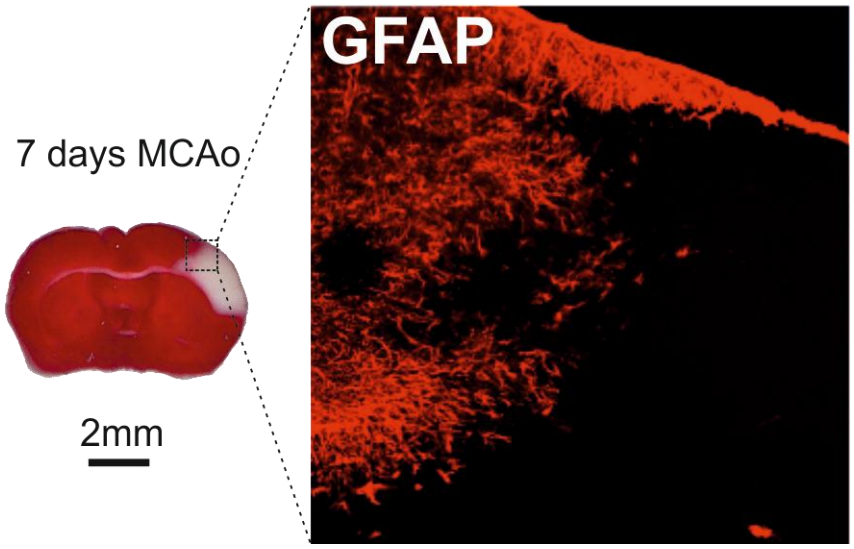

Figure 14. Focal cerebral ischemia leads to a massive astrogliosis around the ischemic core 7 days after MCAo. A coronal brain section stained with triphenyltetrazolium chloride (TTC) indicates the volume of ischemic tissue (white color) 7 days after MCAo. The boxed area shows GFAP overexpression around the ischemic region. MCAo, middle cerebral arthery occlusion; GFAP, glial fibrillary acidic protein.

8.2 Expression of NMDA receptor subunits

To prove the "reactive" properties of astrocytes after ischemia, expression of mRNA encoding GFAP, GFAPδ and vimentin, which are known to be up-regulated in reactive astrocytes (Sofroniew, 2009), was evaluated in control P50 mice and in mice 3, 7 and 14 days after MCAo by high throughput qPCR. As depicted in **Figure 15 and 16**, incidence of astrocytes expressing mRNA for all three proteins (**Fig. 15**) as well as their relative expression (**Fig. 16**) increased dramatically after MCAo with peak of expression 7 days after MCAo.

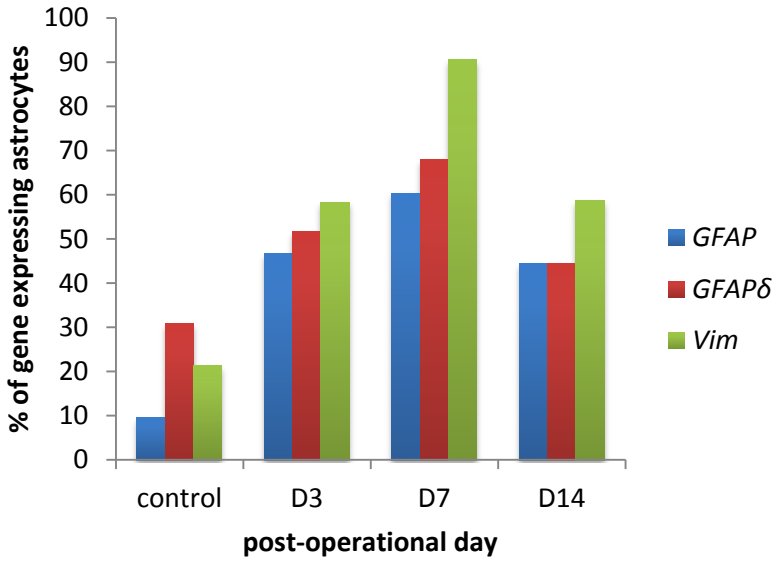

Figure 15. Percentage of astrocytes expressing genes of GFAP, GFAPδ and vimentin in control mice and those after MCAo. Astrocytes isolated from 50 days old mice (control, n=42) and mice 3, 7 and 14 days after MCAo (D3, n=60; D7, n=53; D14, n=63). *GFAP*, glial fibrillary acidic protein; *GFAPδ*, glial fibrillary acidic protein δ; *Vim*, vimentin; D3-14, day 3-14 after MCAo.

The highest increase was observed for vimentin, which was expressed in 21% of astrocytes before MCAo and in 91% of astrocytes 7 days after MCAo. Number of

GFAP-expressing cells increased from 10% to 60% 7 days after MCAo, and GFAPδ expression increased from 31% to 68%.

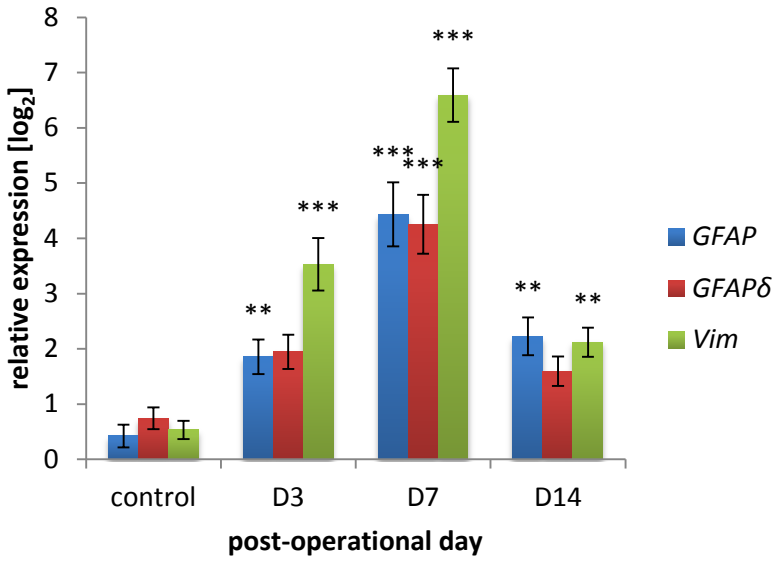

Figure 16. Average relative expression of genes coding GFAP, GFAPδ and vimentin in astrocytes isolated from control mice and those after MCAo. Astrocytes isolated from 50 days old mice (control, n=42) and mice 3, 7 and 14 days after MCAo (D3, n=60; D7, n=53; D14, n=63).). Statistical significance was calculated using one-way ANOVA test where the values after MCAo were compared to the control values; ** p<0.01, very significant; *** p<0.001, extremely significant. *GFAP*, glial fibrillary acidic protein; *GFAPδ*, glial fibrillary acidic protein δ; *Vim*, vimentin; D3-14, day 3-14 after MCAo.

To find out whether astrocytes express NMDA receptor subunits, high throughput qPCR was performed for six genes coding NMDA receptor subunits, namely Grin1, Grin2A-D and Grin3A. Our analysis showed that MCAo results in an increase in the number of astrocytes that express mRNA for all NMDA receptor subunits, with exception for Grin2C (**Fig. 17**). Incidence of the cells expressing gene Grin1 increased gradually from 19% in controls to 48% of the cells isolated 14 days after MCAo (**Fig. 17**). Grin1 encodes GluN1 subunit, which is to current

knowledge obligatory subunit in functional NMDA receptors. Similarly, the amount of astrocytes expressing Grin2A, Grin2B and Grin2D increased during post-ischemic periods. Notably, between 7 and 14 days after ischemic insult, the percentage of astrocytes that express Grin2A and Grin2D increased from 58% to 98% and from 2% to 63%, respectively. In contrast, the number of astrocytes that express Grin2C decreased during first 7 days after MCAo and returned almost to control level 14 days after MCAo (**Fig. 17**).

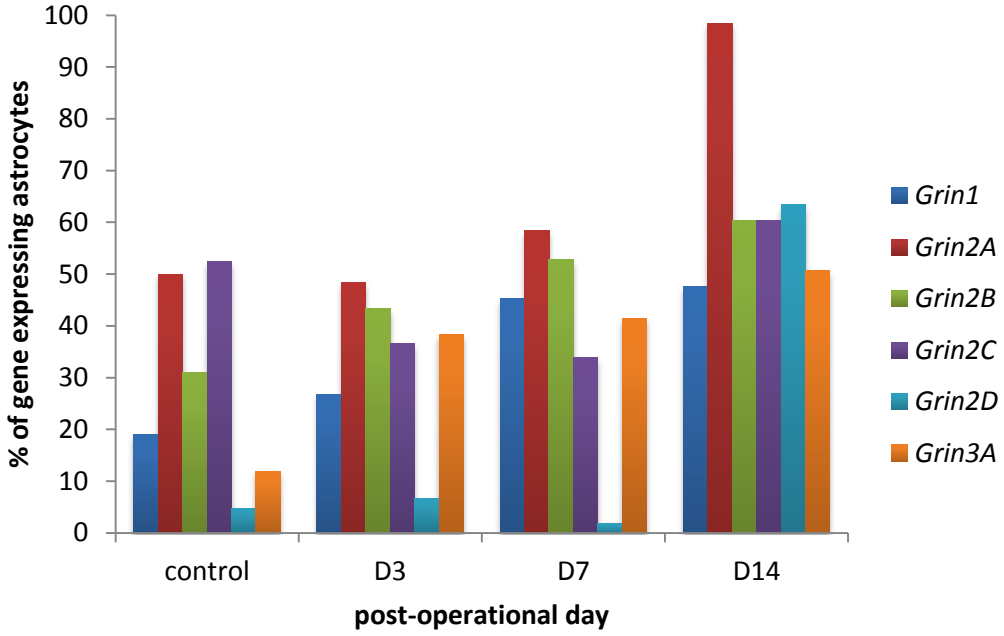

Figure 17. Percentage of astrocytes expressing genes of individual subunits of NMDA receptors in control mice and those after MCAo. Astrocytes isolated from 50 days old mice (control, n=42) and mice 3, 7 and 14 days after MCAo (D3, n=60; D7, n=53; D14, n=63). *Grin1, Grin2A-D, Grin3A*, genes coding individual NMDA receptor subunits; D3-14, day 3-14 after MCAo.

In order to further reveal the expression profile of astrocytes the average relative expression of NMDA receptor subunits was evaluated (**Fig. 18**). Except for Grin2C, the average relative expression of mRNA for each subunit gradually increased after ischemia, which is in perfect correlation with the increasing

amount of astrocytes that expressed individual genes for NMDA receptor subunits (**Fig. 17**). It is worth noting, that Grin2A is the most expressed gene among those coding NMDA receptor subunits. Especially in reactive astrocytes isolated 14 days after MCAo the expression of Grin2A was almost three times higher than the expression of the second most expressed NMDA receptors subunit gene Grin2D (**Fig. 18**).

In summary, reactive astrocytes from the vicinity of ischemic lesion express markedly increased transcript levels of GluN2A, GluN2D and GluN3A subunits of NMDA receptors.

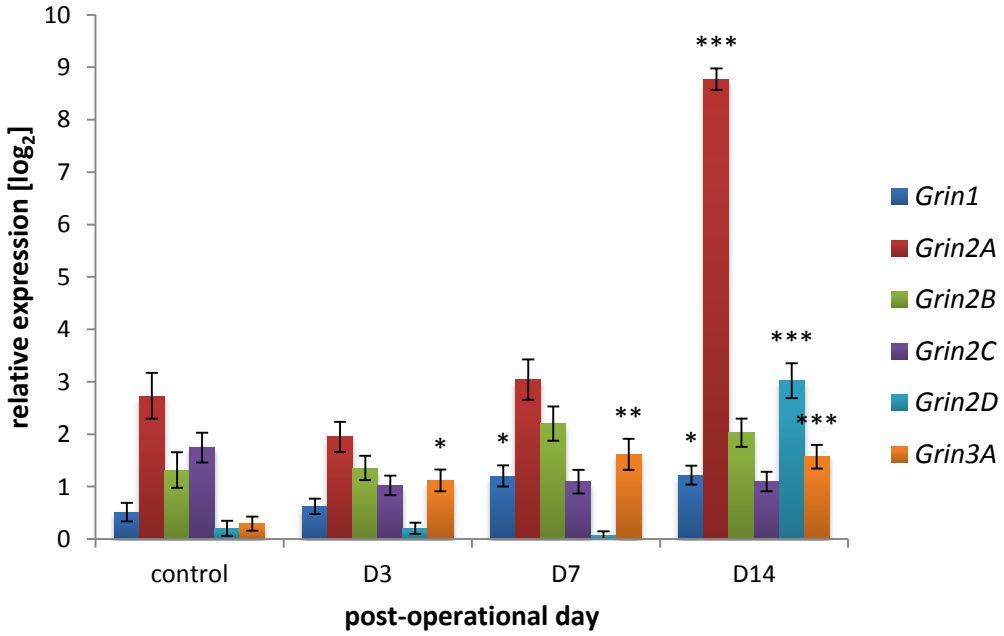

Figure 18. Average relative expression of genes coding individual subunits of NMDA receptors in astrocytes isolated from control mice and those after MCAo. Astrocytes isolated from 50 days old mice (control, n=42) and mice 3, 7 and 14 days after MCAo (D3, n=60; D7, n=53; D14, n=63). Statistical significance was calculated using one-way ANOVA test where the values after MCAo were compared to the control values; * $p<0.05$, significant; ** $p<0.01$, very significant; *** $p<0.001$, extremely significant. *Grin1, Grin2A-D, Grin3A*, genes coding individual NMDA receptor subunits; D3-14, day 3-14 after MCAo.

8.3 Immunohistochemical characterization of NMDA receptor subunits

Based on our gene expression profiling we assumed that the increased number of astrocytes expressing NMDA receptor subunits as well as their increased mRNA levels in individual cells might lead to an increase in protein production in reactive astrocytes. Therefore, we performed immunohistochemical analyses, which revealed marked changes in the expression of NMDA receptor subunits on the protein level following MCAo (**Figures 19, 20 and 21).** We compared stainings of cortical astrocytes for NMDA receptor subunits (GluN1, GluN2A-D and GluN3A) in control mice to those 14 days after MCAo. We found that GluN1 subunit is present only in a few astrocytes in control mice; however, increased GluN1 staining in astrocytes isolated from ischemic mice, indicates that the amount of astrocytes possessing GluN1 subunit rises after ischemia (**Fig. 19**). This correlates well with increased expression of *GriN1* gene after MCAo (**Fig. 17, 18**). Furthermore, we found a similar increase in GluN2D (**Fig. 20**), and especially in GluN3A (**Fig. 19**) immunoreactivity following MCAo, which allowed us to conclude that 14 days after MCAo majority of astrocytes close to the ischemic lesion express these two NMDA receptor subunits. The immunohistochemical staining for GluN2C showed approximately the same amount of astrocytes expressing this subunit prior to and after MCAo (**Fig. 20**), which accords well with comparable expression of *Grin2C* gene in control and ischemic mice (**Fig. 17, 18**). Immunohistochemical staining for GluN2A and GluN2B subunits revealed that there is no overlap of GluN2A and GluN2B immunoreactivity with EGFP fluorescence (**Fig. 21**) suggesting that reactive astrocytes 14 days after MCAo do not express these two subunits. Apart from GluN2A and GluN2B staining, we can conclude that immunohistochemical analysis fully supports results obtained from single cell qPCR study.

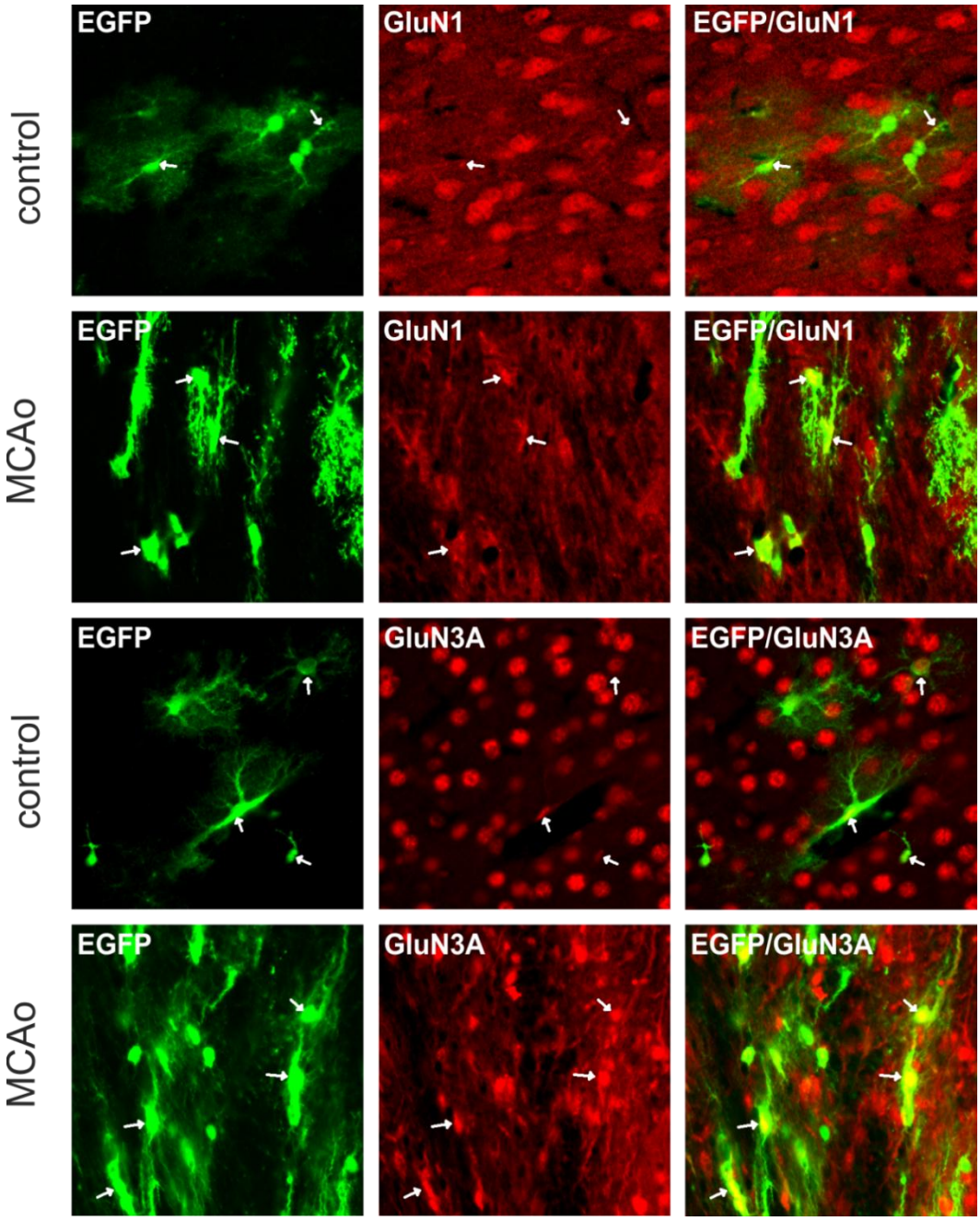

Figure 19. Immunohistochemical analysis of GluN1 and GluN3A subunits of the NMDA receptors in cortical astrocytes of control mice (control) and those 14 days after MCAo (MCAo). Images of coronal slices of the cortex were taken either from uninjured mice (control) or from ipsilateral hemisphere of mice 14 days after MCAo (MCAo). Arrows indicate astrocytes (EGFP-positive) stained for either GluN1 or GluN3A. EGFP, enhanced green fluorescent protein; MCAo, middle cerebral artery occlusion; GluN1 and GluN3A, subunits of NMDA receptors.

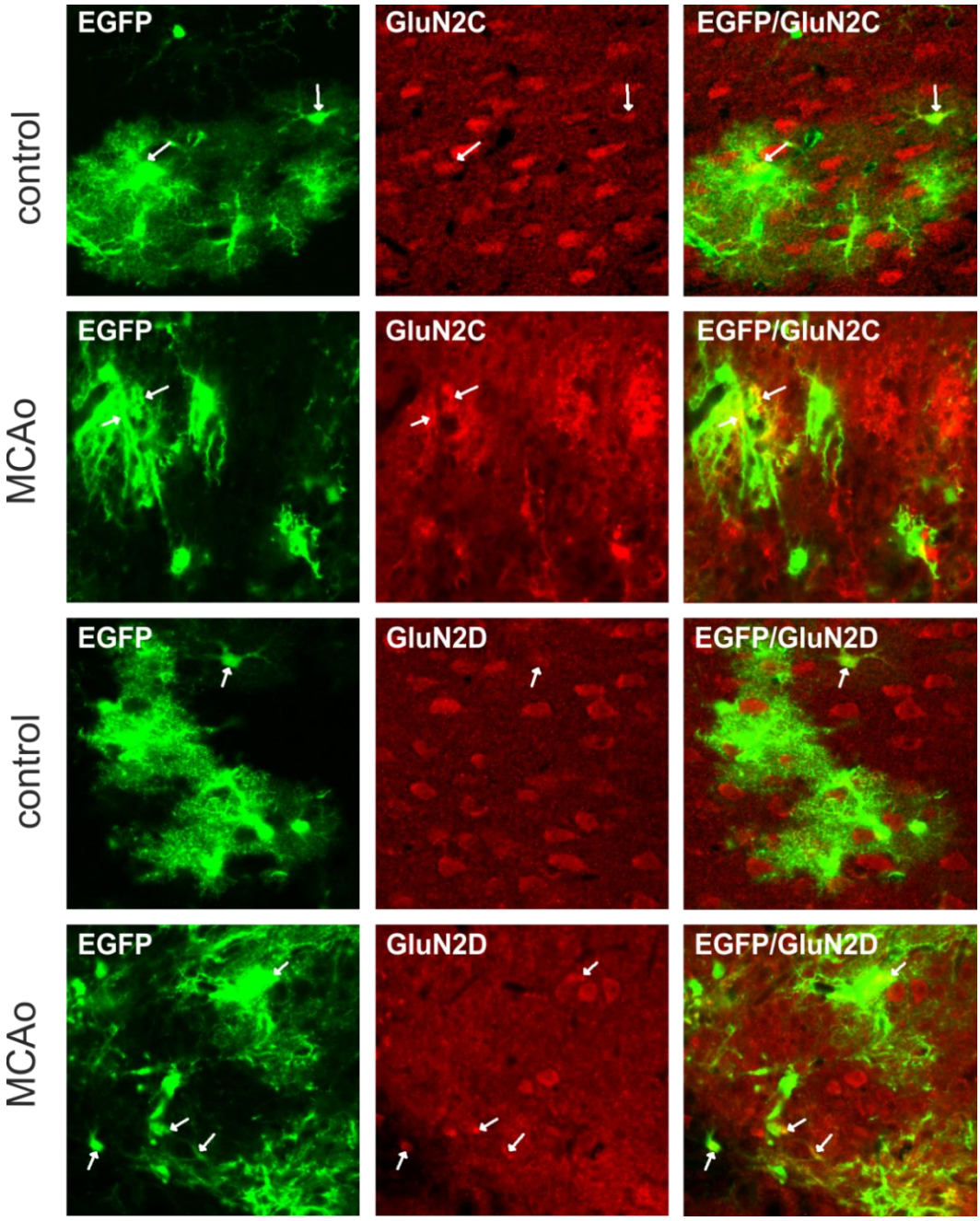

Figure 20. Immunohistochemical analysis of GluN2C and GluN2D subunits of the NMDA receptors in the cortical astrocytes of control mice (control) and those 14 days after MCAo (MCAo). Images of coronal slices of the cortex were taken either from uninjured mice (control) or from ipsilateral hemisphere of mice 14 days after MCAo (MCAo). Arrows indicate astrocytes (EGFP-positive) stained for either GluN2C or GluN2D. EGFP, enhanced green fluorescent protein; MCAo, middle cerebral artery occlusion; GluN2C and GluN2D, subunits of NMDA receptor.

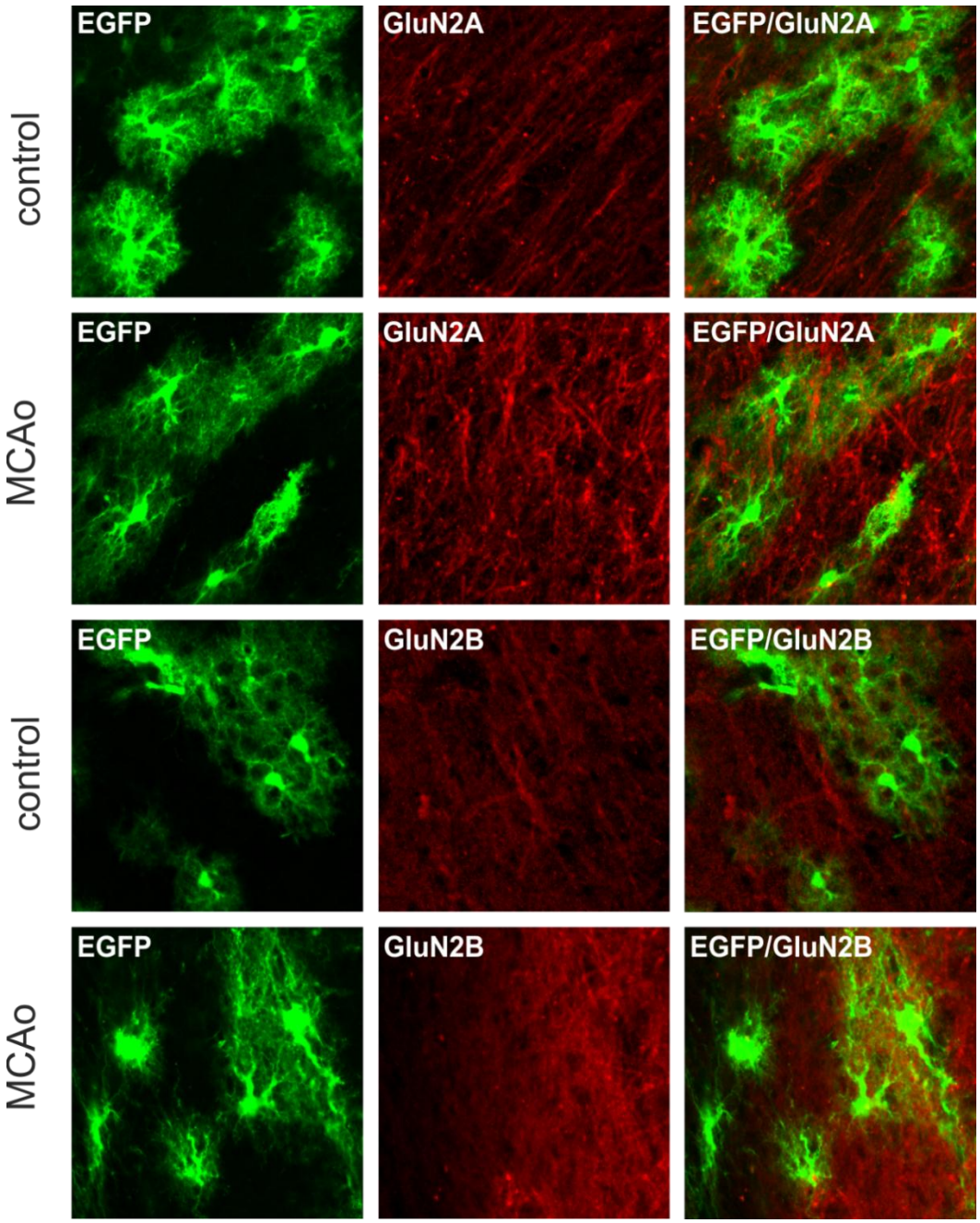

Figure 21. Immunohistochemical analysis of GluN2A and GluN2B subunits of the NMDA receptors in the cortical astrocytes of control mice (control) and those 14 days after MCAo (MCAo). Images of coronal slices of the cortex were taken either from uninjured mice (control) or from ipsilateral hemisphere of mice 14 days after MCAo (MCAo). Arrows indicate astrocytes (EGFP-positive) stained for either GluN2A or GluN2B. EGFP, enhanced green fluorescent protein; MCAo, middle cerebral artery occlusion; GluN2A and GluN2B, subunits of NMDA receptor.

8.4 Electrophysiological characterization of astrocytes

To determine electrophysiological properties of cortical astrocytes, the patch-clamp technique in the whole-cell configuration was employed. **Figure 22** shows characteristic current pattern of astroglial population in tissue slices isolated from control mice - they display large time- and voltage-independent passive K^+ currents in response to membrane hyperpolarization/depolarization from -160 to 40 mV, in 10 mV increments.

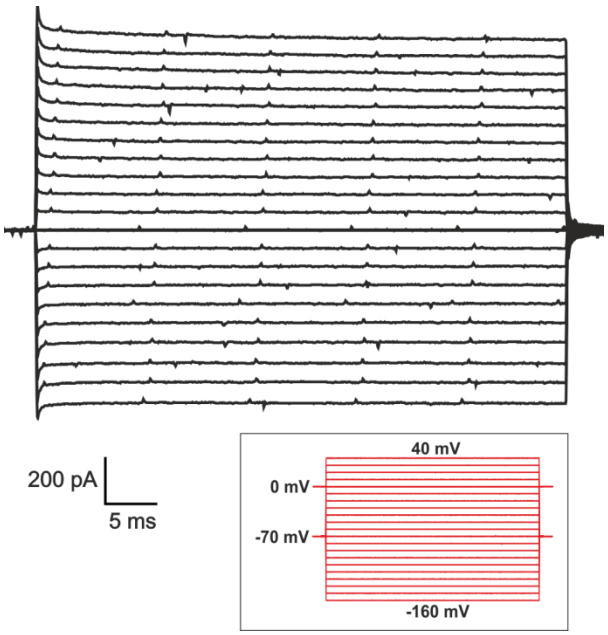

Figure 22. Characteristic current pattern of cortical astroglial population in tissue slices. Astroglial current pattern measured after depolarizing the cell membrane from a holding potential of -70 mV to +40 mV and hyperpolarizing to -160 mV in 10 mV voltage increments. Pulse duration was 50 ms.

In addition to passive conductance, astrocytes also displayed inwardly rectifying K^+ (K_{ir}) currents (**Table 4**). The average astrocytic RMP was -68.7 ± 1.8 mV, membrane resistance (R_m) was 115.4 ± 9.5 MΩ and membrane capacitance was 15.1 ± 3.3 pF (**Table 4**).

The electrophysiological properties of astrocytes in tissue slices isolated from ischemic mice differed significantlly from those of astrocytes isolated from

control animals. Although they also displayed large passive K^+ currents, they were significantly depolarized (RMP = -57.1 ±1.4 mV), they had much lower R_m (75.1 ± 5.7 MΩ) and their C_m increased to 31.8 ± 5.0 pF. The K_{ir} current density of post-ischemic astrocytes almost tripled, reaching 9.1 ± 1.5 pA/pF (**Table 4**).

The membrane properties of cortical astrocytes in tissue slices perfectly fit with the properties of "passive astrocytes" described by Walz (Walz, 2000).

Table 4. Electrophysiological properties of cortical astrocytes in tissue slices isolated from control mice (control) and those 13-28 days after MCAo (MCAo)

		control			MCAo		
		average	S.E.M	n	average	S.E.M	n
RMP	[mV]	-68.7	1.8	32	-57.1***	1.4	29
R_m	[MΩ]	115.4	9.5	32	75.1***	5.7	29
C_m	[pF]	15.1	3.3	32	31.8*	5.0	29
K_{ir}/C_m	[pA/pF]	3.5	1.4	32	9.1*	1.5	29
K_a/C_m	[pA/pF]	-	-	32	-	-	29
K_{dr}/C_m	[pA/pF]	-	-	32	-	-	29

MCAo, middle cerebral artery occlusion; RMP, resting membrane potential; R_m, membrane resistance; C_m, membrane capacitance; K_{ir}/C_m, current density of inwardly-rectifying K^+ currents; K_a/C_m, current density of the fast activating and inactivating outwardly-rectifying K^+ currents; K_{dr}/C_m, current density of voltage-gated delayed outwardly-rectifying K^+ currents; S.E.M., standard error of the mean. Statistical significance was calculated using one way ANOVA test; * $p<0.05$, significant; ** $p<0.01$, very significant; *** $p<0.001$, extremely significant.

Membrane properties of astrocytes isolated from the cortex of P50 mice and cultured for 3-5 days differed from those recorded in the brain slices. They displayed characteristic properties of "complex" astrocytes described previously (Walz, 2000) - in addition to passive conductance and K_{ir} currents, they also displayed K_{dr} and K_a currents (**Table 5**). Apart from expression of voltage-gated K^+ channels, cultured astrocytes had more positive RMP (-61.9 ± 4.3 mV) and higher

R_m (221.3 ± 32.7 MΩ) and C_m (39.2 ± 14.3 pF) when compared to astrocytes in tissue slices prepared from non-injured mice (**Table 5**).

Table 5. Electrophysiological properties of astrocytes isolated from the cortex of control mice and cultured for 3-5 days.

		average	S.E.M.	n
RMP	[mV]	-61.9	4.3	21
R_m	[MΩ]	221.3	32.7	21
C_m	[pF]	39.2	14.3	21
K_{ir}/C_m	[pA/pF]	4.7	1.0	21
K_a/C_m	[pA/pF]	5.0	3.4	21
K_{dr}/C_m	[pA/pF]	10.3	4.1	21

RMP, resting membrane potential; R_m, membrane resistance; C_m, membrane capacitance; K_{ir}/C_m, current density of inwardly-rectifying K^+ currents; K_a/C_m, current density of the fast activating and inactivating outwardly-rectifying K^+ currents; K_{dr}/C_m, current density of voltage-gated delayed outwardly-rectifying K^+ currents; S.E.M., standard error of the mean.

8.5 Function of astroglial NMDA receptors: intracellular Ca^{2+}-imaging

Based on the results obtained from single cell qPCR and immunohistochemical analyses, we performed the functional study of astroglial NMDA receptors using intracellular Ca^{2+}-imaging technique. For our experiments we used cultured astrocytes as well as tissue slices prepared from control mice and mice 13-28 days after MCAo. *In vitro* measurements were performed in astrocytes isolated from controls, (n=26 cells), as well as those isolated from the vicinity of ischemic lesion (n=47 cells). Surprisingly, no intracellular Ca^{2+} elevation was detected in cultured astrocytes in response to application of 100 µM NMDA.

In contrast to *in vitro* measurements, experiments performed in tissue slices revealed interesting results. **Figure 23** shows representative fluorescence

traces of intracellular Ca^{2+} elevations evoked by two NMDA receptor agonists, glycine and NMDA.

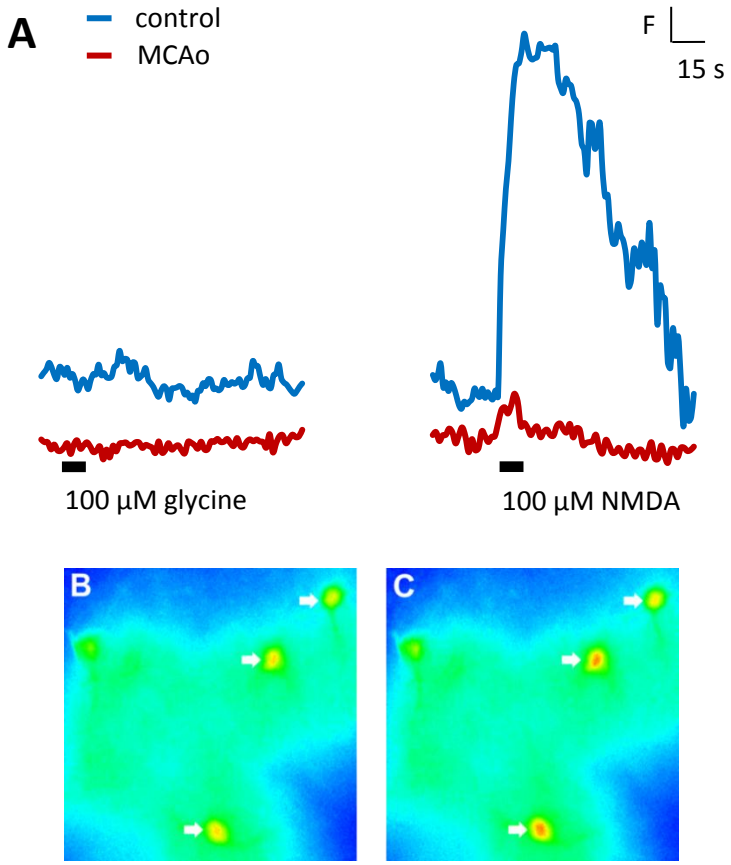

Figure 23. Intracellular Ca^{2+}-imaging. A) Representative fluorescenct traces of intracellular Ca^{2+} elevations in mouse cortical astrocytes after application of 100 µM glycine and 100 µM NMDA. Astrocytes isolated from 50 days old mice (control, n=24) and mice 13-28 days after MCAo (MCAo, n=32). **B, C)** Fluorescent signal of Oregon Green BAPTA-1 prior to **(B)** and in response to application of 100 µM NMDA **(C).** Arrows indicate astrocytes responding to application of 100 µM NMDA. NMDA, N-methyl-D-aspartate; MCAo, middle cerebral arthery occlusion; F, fluorescence; s, second.

It is obvious that application of 100 µM glycine did not evoke any intracellular Ca^{2+} elevation in control or ischemic astrocytes; however, application of 100 µM NMDA triggered an increase in intracellular Ca^{2+} concentration in control astrocytes, while no response was detected in astrocytes isolated from the ischemic regions (**Fig. 23**).

To rule out the possibility that the Ca^{2+} elevations in astrocytes were just indirect effect of neuronal activity upon NMDA application, the experiments were repeated with 100 µM NMDA in the presence of 1 µM TTX, which functions as voltage-gated Na^{+} channel blocker (Narahashi, 2008). Since no significant changes in the number of responding astrocytes (**Fig. 24**) as well as in the amplitude of NMDA-specific responses (**Fig. 25**) were observed, our findings indicate that intracellular Ca^{2+} elevations in astrocytes are triggered by activation of astroglial NMDA receptors rather than by indirect neuronal activity.

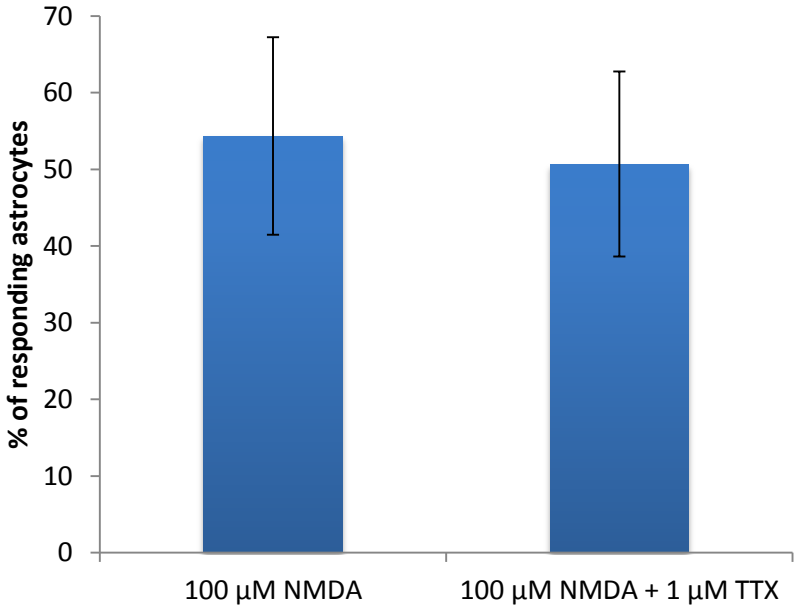

Figure 24. Percentage of astrocytes isolated from control mice responding to application of 100 µM NMDA or 100 µM NMDA in the presence of 1 µM TTX. Astrocytes isolated from 50 days old mice (n=55)**.** NMDA, N-methyl-D-aspartate; TTX, tetrodotoxin.

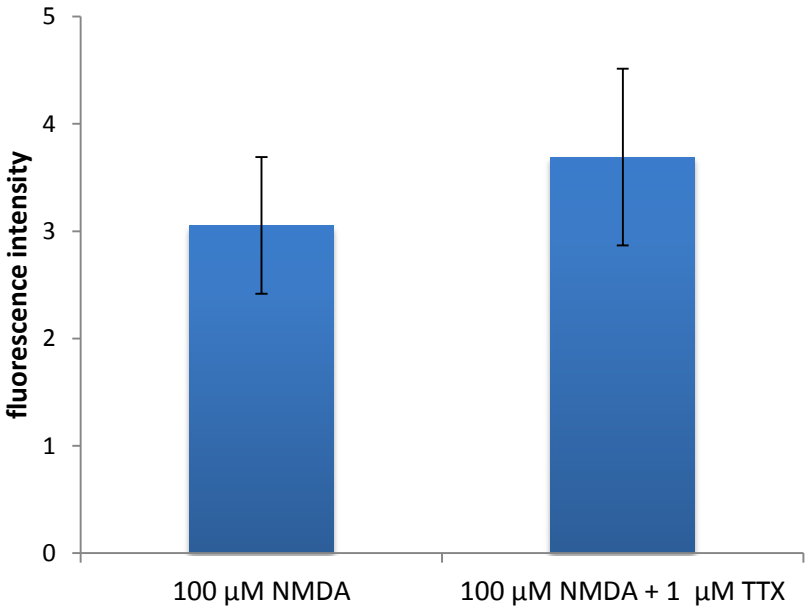

Figure 25. Changes in fluorescence intensities evoked by application of 100 µM NMDA or 100 µM NMDA in the presence of 1 µM TTX in astrocytes isolated from control mice. Astrocytes isolated from 50 days old mice (n=55)**.** NMDA, N-methyl-D-aspartate; TTX, tetrodotoxin.

The single-cell qPCR as well as immunohistochemical analyses suggested that not all astrocytes possess NMDA receptors, which was confirmed also by Ca^{2+}-imaging study. Although glycine application did not trigger intracellular Ca^{2+} increase in astrocytes from control or ischemic mice, application of NMDA induced intracellular Ca^{2+} elevation in 58% of analyzed astrocytes in control mice (**Fig. 26A**). In contrast to qPCR and immunohistochemical results, which showed increased expression of NMDA receptors in ischemic astrocytes, the amount of astrocytes isolated from mice after MCAo that respond to NMDA application, decreased to 16% (**Fig. 26A**). Together with decreased number of astrocytes responding to NMDA application, we observed also a decrease in amplitude of NMDA-evoked responses (**Fig. 26B**).

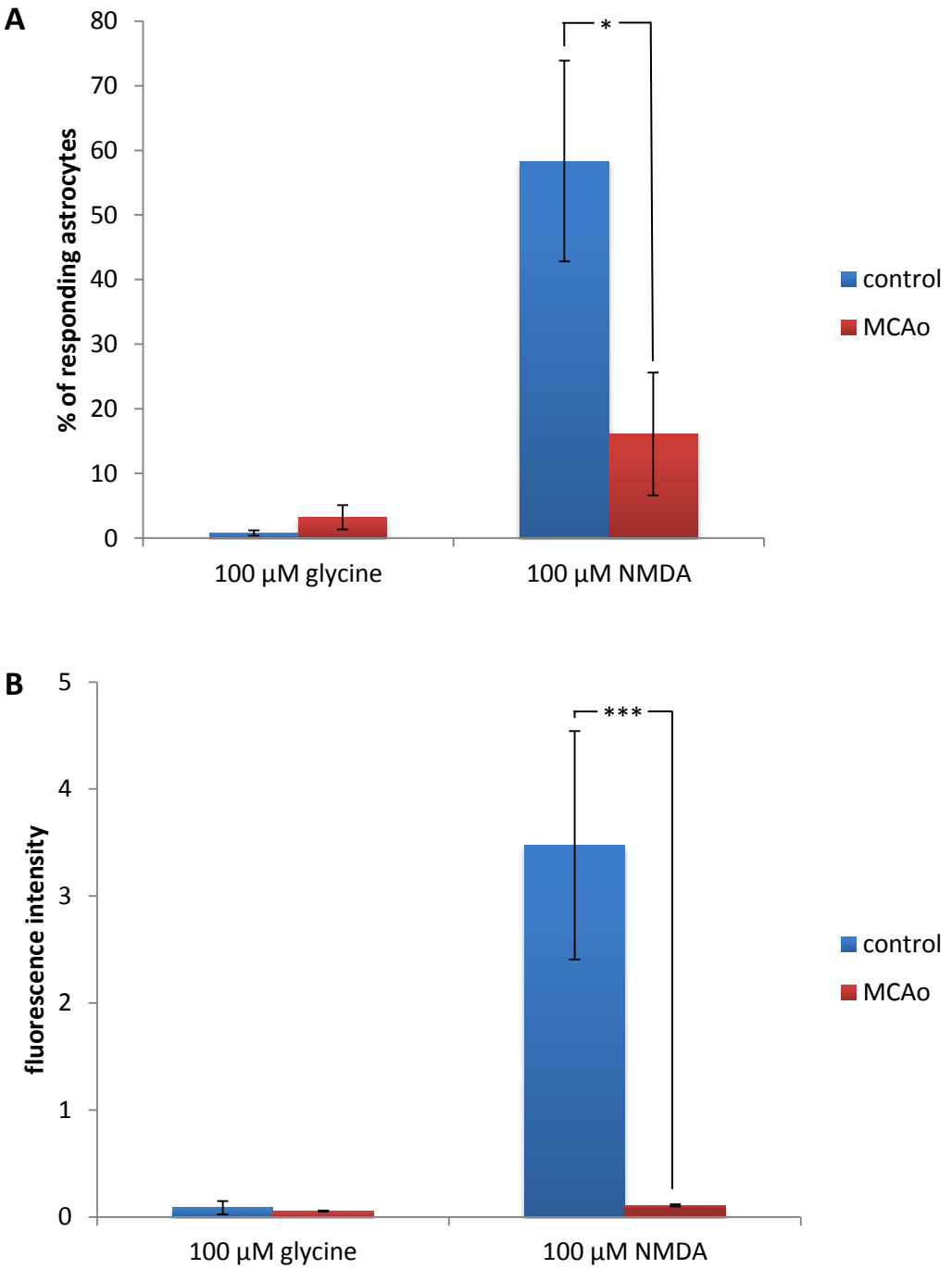

Figure 26. A) Percentage of astrocytes responding to application of 100 µM glycine and 100 µM NMDA in control mice and those after MCAo and respective changes in fluorescence intensities (B). Astrocytes isolated from 50 days old mice (control, n=24) and mice 13-28 days after MCAo (MCAo, n=32). Statistical significance was calculated using one-way ANOVA test; * $p < 0.05$ significant; *** $p<0.001$, extremely significant. NMDA, N-methyl-D-aspartate; MCAo, middle cerebral artery occlusion.

9 DISCUSSION

In present study we used the GFAP/EGFP mice to study function and expression profile of NMDA receptors in cortical astrocytes after ischemic insult. Traditionally, the studies on NMDA receptors were mainly focused on neurons. Currently, there are several works concerning NMDA receptors in astrocytes (Akazawa et al., 1994; Conti et al., 1996, 1999; Latour et al., 2001; Lalo et al., 2006, 2011a; Lee et al., 2010; Palygin et al., 2010, 2011; Zhou et al., 2010) and only three works that examined their role in astrocytes in the context of cerebral ischemia (Gottlieb and Matute, 1997; Krebs et al., 2003; Zhou et al., 2010). On the basis of our results obtained from single-cell qPCR and immunohistochemical analyses, here we report, for the first time, that cortical astrocytes express all NMDA receptor subunits GluN1, GluN2A-D and GluN3A and that their expression is dramatically altered after MCAo (**Fig. 17, 18, 19, 20**). Furthermore functional studies employing intracellular Ca^{2+}-imaging revealed that Ca^{2+} permeability of astroglial NMDA receptors is markedly attenuated after MCAo (**Fig. 23, 26**).

To elucidate the influence of focal ischemia on the astroglial NMDA receptors we use microsurgically-induced distal MCAo, the well reproducible animal model of stroke (Kuraoka et al., 2009). In accordance with previous works, the injured area of the brain was restricted almost exclusively to the cortical regions (**Fig. 14**) unlike intraluminal monofilament MCAo, which produce severe hemispheric ischemia involving thalamic and hypothalamic regions (Carmichael, 2005; Kuraoka et al., 2009). The infarct lesion was surrounded by massive glial scar, the hallmark of majority of brain injuries such as trauma, ischemia or neurodegeneration (Pekny and Nilsson, 2005). The glial scar was formed particularly by reactive astrocytes, which were characterized by increased production of intermediate filaments GFAP and vimentin, which were reported to be up-regulated in reactive astrocytes in response to various brain injuries including ischemia (**Fig. 14, 15, 16**) (Pekny and Pekna, 2004).

Together with increased production of GFAP and vimentin, we also observed an increase in the number of cortical astrocytes that expressed mRNA of genes coding NMDA receptor subunits GluN1, GluN2A-D and GluN3A (**Fig. 17**), as well as an increase in mRNAs levels of these genes in individual cells (**Fig. 18**) following MCAo.

Only few studies regarding the expression of NMDA receptor subunits in cortical astrocytes at the transcript level were published (Conti et al., 1994; Schipke et al., 2001; Cahoy et al., 2008), but none of them showed the expression of all NMDA receptors subunits. In 1994 Conti and colleagues failed in detection of GluN1 subunit in rat cortical astrocytes by in situ hybridization (Conti et al., 1994). In accordance with our results, Schipke and co-workers proved the expression of GluN1, GluN2B and GluN2C in mouse cortical astrocytes by RT-PCR, but did not detect GluN2A, GluN2D and GluN3 (Schipke et al., 2001). The latest work that demonstrated the presence of mRNA for NMDA receptor subunits in mouse cortical astrocytes were performed by Cahoy and co-authors (Cahoy et al., 2008). Using Affymetrix GeneChip microarrays they did not detect transcripts for GluN1 subunit, but they reported high mRNA levels for GluN2C and GluN3A subunits in cortical astrocytes. The discrepancy among presented results may be caused by many factors such as type of transgenic mice, the animals' age or the method employed for analysis. For example, in our experiments, we used 40-60-day-old mice, while in the other two mentioned studies rather young animals were used; P1-P17 mice (Cahoy et al., 2008) and P7-P28 mice (Schipke et al., 2001). Moreover, Schipke and colleagues used GFAP/EGFP transgenic mice to identify the astroglial population, while Cahoy and co-workers used transgenic mice, in which astrocytes were labeled by the EGFP, which expression was under the control of S100 calcium binding protein β promotor. The difference in genetic-based sorting criteria could lead to isolation of different astrocyte sub-populations and in turn cause inconsistency of obtained results.

To the best of our knowledge, there is no study to compare our results showing marked increase in expression of NMDA receptor subunits in acutely isolated cortical astrocytes after MCAo. Only Zhou and co-authors detected significant up-regulation of mRNAs encoding GluN1 and GluN2B subunits 2 hours after OGD in cultured cortical astrocytes, while mRNA coding GluN2A was down-regulated 6 hours after OGD (Zhou et al., 2010). In contrast to our results, a decrease in the expression of genes encoding GluN1, GluN2A and GluN2B was reported in hippocampal neurons 7 days after ischemia (Liu et al., 2010)

Up to now, only GluN1 (Aoki et al., 1994; Conti et al., 1996), GluN2A and GluN2B (Conti et al., 1996) subunits were detected in murine cortical astrocytes by immunohistochemistry. Here we report the presence of GluN1, GluN2C, GluN2D and GluN3A at the protein level in cortical astrocytes in tissue slices isolated from control mice. Furthermore, we detected marked increase in the number of cortical astrocytes that possess all mentioned subunits 14 days after MCAo (**Fig. 19, 20**), which is in accord with our single-cell qPCR results, with the exception for GluN2A and GluN2B subunits.

GluN1 subunit is considered to be essential component of functional NMDA receptor (Paoletti and Neyton, 2007). The up-regulation of mRNA that encodes GluN1 together with increased GluN1-immunoreactivity of the astrocytes might indicate that ischemia induces quite high density of functional NMDA receptors in cortical astrocytes. Very intriguing is the observed increase in the number of astrocytes expressing GluN2D and GluN3A (**Fig. 19, 20**). It was shown that brains of neonate mammals, which are more tolerant to hypoxia than adult mammals' brains, as well as the brains of some hypoxia-tolerant species such as the subterranean mole-rat or *Spalax*, contain NMDA receptors with higher representation of GluN2D subunits (Band et al., 2012; Peterson et al., 2012). Insertion of GluN2D causes reduction of open time probability of the NMDA receptors under hypoxic condition when compared to the NMDA receptors without this subunit in neurons. Consequently, less Ca^{2+} can enters the cell

resulting in attenuating Ca^{2+}-mediated cell damage (Bickler et al., 2003). GluN3A subunit is referred to be a dominant negative modulator of NMDA receptors. The presence of GluN3A dramatically reduces Ca^{2+} permeability, unitary conductance, current amplitude and open probability of NMDA receptors, which leads to lower Ca^{2+} entry through GluN3A-containing receptors and therefore GluN3A subunit is supposed to be neuroprotective (Henson et al., 2010; Pachernegg et al., 2012). Moreover, it was reported that GluN3A-mediated neuroprotection is associated with inhibition of calpains, the Ca^{2+}-dependent proteases (Martínez-Turrillas et al., 2012). Taken together, we hypothesize that presence of high levels of GluN2D and GluN3A subunits in astrocytes following ischemia could play a role in protection of astrocytes against glutamate excitotoxicity.

The results obtained from single-cell qPCR and immunohistochemical analyses for GluN2A and GluN2B subunits are controversial (**Fig. 17, 18, 21**). Although the number of astrocytes that express mRNA for GluN2A and GluN2B subunits as well as the relative expression of these subunits increased after MCAo (especially in the case of GluN2A), we were unable to detect them by immunohistochemical staining in controls or ischemic mice. Conti and colleagues (Conti et al., 1996), who proposed the presence of GluN2A and GluN2B in cortical astrocytes used rats in their studies, which might be the cause of discrepancies between their and our results. It was shown previously that ischemia induces the specific enzymatic cleavage of GluN2A C-terminus in neurons, which prevents the detection of GluN2A by antibodies directed against this region (Gascón et al., 2008).Therefore the absence of GluN2A subunit staining following MCAo, could be caused by the fact that our antibody is directed against C-terminal region of GluN2A. Nonetheless, it is also possible that antibodies employed during our experiments are not sufficient for detecting GluN2A and GluN2B subunits and new antibodies should be considered.

The electrophysiological properties of cortical astrocytes were evaluated using patch-clamp technique. We showed that cortical astrocytes display large passive K^+ currents and characteristic membrane properties of ‘’passive’’ astrocytes described previously (**Fig. 22**) (Walz, 2000; Isokawa and McKhann, 2005; Pivonkova et al., 2010; Butenko et al., 2012). In accordance with previous studies (Pivonkova et al., 2010; Butenko et al., 2012), we also showed that astrocytes from the vicinity of ischemic lesion are depolarized and show increased current density of K_{ir} when compared to astrocytes in control mice (**Table 4**). Astrocytes isolated from control mice and cultured for 3-5 days markedly differed from those in brain slices. Confirming previous results (Butenko et al., 2012), they displayed higher R_m and RMP and in contrast to astrocytes in tissue slices they had ”complex” current pattern represented by presence of K_a and K_{dr} (**Table 5**)(Walz, 2000; Isokawa and McKhann, 2005). These currents are developmentally regulated and their contribution decreases during maturation. Furthermore K_{dr} and K_a are considered as indirect markers of precursor cells by some authors (Walz, 2000), suggesting that some astrocytes in cultures undergone dedifferentiation to become the progenitor cells or immature astrocytes.

Our intracellular Ca^{2+}-imaging studies performed in vitro, on astrocytes isolated from cortex of controls and ischemic mice and cultured for 3-5 days, confirmed the results of earlier studies (Holzwarth et al., 1994; Kato et al., 2006) showing that application of NMDA does not trigger intracellular Ca^{2+} elevation in these cells. This may be a result of the enzymatic treatment of cells during cultures preparation, which was reported to inhibit the NMDA-evoked currents in cultured neurons (Akaike et al., 1988; Allen et al., 1988).

In contrast to experiments performed on cultured cells, our Ca^{2+}-imaging data obtained from astrocytes in brain slices confirmed the previously described NMDA-evoked intracellular Ca^{2+} rises in cortical astrocytes in situ (Schipke et al., 2001; Palygin et al., 2010, 2011) and they accord well with our single-cell qPCR

and immunohistochemical analysis that showed presence of NMDA receptors in astrocytes. In cortical astrocytes of ischemic mice we observed marked decrease in the number of astrocytes, which displayed Ca^{2+} elevations in response to application of NMDA as well as in the amplitude of NMDA-specific responses (**Fig. 23, 26**). It might looks peculiar that despite of increased expression of individual NMDA receptor subunits at the transcript and protein levels, the responses evoked by application of NMDA were lower after MCAo. However, one has to consider the facts described above, namely that GluN2D and GluN3A subunits, which are the most expressed among all NMDA receptor subunits at protein levels after MCAo, make the Ca^{2+} entry through NMDA receptors highly unlikely (Bickler et al., 2003; Henson et al., 2010; Pachernegg et al., 2012). Moreover the presence of both these subunits considerably reduces Ca^{2+}/ Na^{+} conductance as well as open probability of NMDA receptors, which might reduce further cell damage (Won et al., 2002; Onténiente et al., 2003). In contrast to neurons, which significantly reduce the expression of NMDA receptors after ischemia to prevent influx of cations and to reduce cellular damage (Gascón et al., 2008; Liu et al., 2010), astrocytes markedly increase production of all NMDA receptors subunits in response to ischemia. Taken together, it seems that increased NMDA receptor activity in reactive astrocytes does not have damaging effect, but it is possibily designated for another purpose, which could explain the apparent illogicality of increasing expression of NMDA receptors in astrocytes after MCAo.

If we admit that astroglial NMDA receptors following ischemia have not primarily damaging effect, it is obvious that they must play another important role. As was described in the section 3.5, influx of Na^{+} into astrocytes has variety of consequences. For example, Na^{+} influx stimulates function of Na^{+}/K^{+}-ATPase, and therefore results in lowering the extracellular K^{+} concentration, which leads to diminishing the depolarizing effect of high extracellular K^{+} concentration on neuronal membrane. Moreover, the increase in Na^{+}/K^{+}-ATPase activity

stimulates aerobic glycolysis and in turn production of lactate that can serve as metabolic substrate for damaged neurons (Lalo et al., 2011b). Furthermore, NMDA receptors are not just ion channels. They are coupled to a variety of downstream effectors, some of which produce survival promoting signals. NMDA receptors are coupled to nitric oxide synthase, which produces nitric oxide, the well-known vasodilator that could improve blood supply of ischemic regions. NMDA receptors are also coupled to certain kinases, such as protein kinase B, extracellular signal-regulated kinase 1 or calmodulin kinase. These kinases can activates some pro-survival transcriptional factors, such as cyclic-adenosin monophosphate response element-binding protein (CREB) or nuclear factor kappa-light-chain-enhancer of activated B cells (NF-κB), which control transcription of some apoptotic inhibitors (B-cell lymphoma protein) and neurotrophic factors like brain-derived neurotrophic factor (Hetman and Kharebava, 2006).

Taken together, the role of astroglial NMDA receptors in ischemic brain tissue remains elusive, but based on our results we propose a novel potential role of astroglial NMDA receptors that lies in mediating protective signals to damage tissue.

10 Conclusion

In summary, we have shown that under physiological conditions astrocytes in adult mouse cortex express all subunits necessary for functional NMDA receptor formation. Although the expression of functional NMDA receptors in mouse cortical astrocytes was reported earlier (Schipke et al., 2001; Palygin et al., 2010, 2011), here we show for the first time, that the expression profile as well as functional properties of astroglial NMDA receptors change dramatically following cerebral ischemia, indicating their involvement in astrocytic response to ischemia.

The increased production of NMDA receptors was surprisingly accompanied by significant reduction of Ca^{2+} entry into astrocytes in response to application of NMDA following ischemic insult. Since influx of Ca^{2+} ions and consequent modulation of many Ca^{2+}-dependent effectors is generally associated with NMDA receptor function, our results suggest a new conception of Ca^{2+}-independent NMDA receptors-mediated signaling in astrocytes following cerebral ischemia and present a new molecular target to be explored in order to define astrocyte-mediated signaling in pathogenesis of acute brain disorders.

Abramov AY, Scorziello A, Duchen MR (2007) Three distinct mechanisms generate oxygen free radicals in neurons and contribute to cell death during anoxia and reoxygenation. The Journal of neuroscience : the official journal of the Society for Neuroscience 27:1129–1138.

Akaike N, Kaneda M, Hori N, Krishtal OA (1988) Blockade of N-methyl-D-aspartate response in enzyme-treated rat hippocampal neurons. Neuroscience letters 87:75–79.

Akazawa C, Shigemoto R, Bessho Y, Nakanishi S, Mizuno N (1994) Differential expression of five N-methyl-D-aspartate receptor subunit mRNAs in the cerebellum of developing and adult rats. The Journal of comparative neurology 347:150–160.

Allen CN, Brady R, Swann J, Hori N, Carpenter DO (1988) N-methyl-D-aspartate (NMDA) receptors are inactivated by trypsin. Brain research 458:147–150.

Allen NJ, Barres BA (2009) Neuroscience: Glia - more than just brain glue. Nature 457:675–677.

Amiry-Moghaddam M, Ottersen OP (2003) The molecular basis of water transport in the brain. Nature reviews Neuroscience 4:991–1001.

Aoki C, Venkatesan C, Go CG, Mong JA, Dawson TM (1994) Cellular and subcellular localization of NMDA-R1 subunit immunoreactivity in the visual cortex of adult and neonatal rats. The Journal of neuroscience : the official journal of the Society for Neuroscience 14:5202–5222.

Araque A, Parpura V, Sanzgiri RP, Haydon PG (1999) Tripartite synapses: glia, the unacknowledged partner. Trends in neurosciences 22:208–215.

Astrup J, Siesjo BK, Symon L (1981) Thresholds in cerebral ischemia - the ischemic penumbra. Stroke 12:723–725.

Band M, Malik A, Joel A, Avivi A (2012) Hypoxia associated NMDA receptor 2 subunit composition: developmental comparison between the hypoxia-tolerant subterranean mole-rat, Spalax, and the hypoxia-sensitive rat. Journal of comparative physiology B, Biochemical, systemic, and environmental physiology 182:961–969.

Bickler P., Fahlman C., Taylor D. (2003) Oxygen sensitivity of NMDA receptors: relationship to NR2 subunit composition and hypoxia tolerance of neonatal neurons. Neuroscience 118:25–35.

Blakeley JO, Llinas RH (2007) Thrombolytic therapy for acute ischemic stroke. Journal of the neurological sciences 261:55–62.

Bowman CL, Kimelberg HK (1984) Excitatory amino acids directly depolarize rat brain astrocytes in primary culture. Nature 311:656–659.

Bushong E a, Martone ME, Jones YZ, Ellisman MH (2002) Protoplasmic astrocytes in CA1 stratum radiatum occupy separate anatomical domains. The Journal of neuroscience : the official journal of the Society for Neuroscience 22:183–192.

Butenko O, Dzamba D, Benesova J, Honsa P, Benfenati V, Rusnakova V, Ferroni S, Anderova M (2012) The increased activity of TRPV4 channel in the

astrocytes of the adult rat hippocampus after cerebral hypoxia/ischemia. PloS one 7:e39959.

Cahoy JD, Emery B, Kaushal A, Foo LC, Zamanian JL, Christopherson KS, Xing Y, Lubischer JL, Krieg P a, Krupenko S a, Thompson WJ, Barres B a (2008) A transcriptome database for astrocytes, neurons, and oligodendrocytes: a new resource for understanding brain development and function. The Journal of neuroscience : the official journal of the Society for Neuroscience 28:264–278.

Cannon JG (1985) Fundamentals of neuropsychopharmacology. By Robert S. Feldman and Linda F. Quenzer. Sinauer Associates, Sunderland, MA 01375. 1984. 508 pp. 19.5 × 24 cm. $35.00. Journal of Pharmaceutical Sciences 74:800–800.

Carmichael ST (2005) Rodent models of focal stroke: size, mechanism, and purpose. NeuroRx : the journal of the American Society for Experimental NeuroTherapeutics 2:396–409.

Conti F, Barbaresi P, Melone M, Ducati a (1999) Neuronal and glial localization of NR1 and NR2A/B subunits of the NMDA receptor in the human cerebral cortex. Cerebral cortex (New York, NY : 1991) 9:110–120.

Conti F, DeBiasi S, Minelli a, Melone M (1996) Expression of NR1 and NR2A/B subunits of the NMDA receptor in cortical astrocytes. Glia 17:254–258.

Conti F, Minelli A, Molnar M, Brecha NC (1994) Cellular localization and laminar distribution of NMDAR1 mRNA in the rat cerebral cortex. The Journal of comparative neurology 343:554–565.

Contreras JE, Sánchez HA, Véliz LP, Bukauskas FF, Bennett MVL, Sáez JC (2004) Role of connexin-based gap junction channels and hemichannels in ischemia-induced cell death in nervous tissue. Brain research Brain research reviews 47:290–303.

Danton GH, Dietrich WD (2004) The search for neuroprotective strategies in stroke. AJNR American journal of neuroradiology 25:181–194.

Eid T, Lee T-SW, Thomas MJ, Amiry-Moghaddam M, Bjørnsen LP, Spencer DD, Agre P, Ottersen OP, De Lanerolle NC (2005) Loss of perivascular aquaporin 4 may underlie deficient water and K+ homeostasis in the human epileptogenic hippocampus. Proceedings of the National Academy of Sciences of the United States of America 102:1193–1198.

Emsley JG, Macklis JD (2006) Astroglial heterogeneity closely reflects the neuronal-defined anatomy of the adult murine CNS. Neuron glia biology 2:175–186.

Feustel PJ, Jin Y, Kimelberg HK (2004) Volume-regulated anion channels are the predominant contributors to release of excitatory amino acids in the ischemic cortical penumbra. Stroke; a journal of cerebral circulation 35:1164–1168.

Gascón S, Sobrado M, Roda JM, Rodríguez-Peña a, Díaz-Guerra M (2008) Excitotoxicity and focal cerebral ischemia induce truncation of the NR2A and

NR2B subunits of the NMDA receptor and cleavage of the scaffolding protein PSD-95. Molecular psychiatry 13:99–114.

Gottlieb M, Matute C (1997) Expression of ionotropic glutamate receptor subunits in glial cells of the hippocampal CA1 area following transient forebrain ischemia. Journal of cerebral blood flow and metabolism : official journal of the International Society of Cerebral Blood Flow and Metabolism 17:290–300.

Halassa MM, Fellin T, Takano H, Dong J-H, Haydon PG (2007) Synaptic islands defined by the territory of a single astrocyte. The Journal of neuroscience : the official journal of the Society for Neuroscience 27:6473–6477.

Hamann M, Rossi DJ, Marie H, Attwell D (2002) Knocking out the glial glutamate transporter GLT-1 reduces glutamate uptake but does not affect hippocampal glutamate dynamics in early simulated ischaemia. The European journal of neuroscience 15:308–314.

Hamill OP, Marty A, Neher E, Sakmann B, Sigworth FJ (1981) Improved patch-clamp techniques for high-resolution current recording from cells and cell-free membrane patches. Pflügers Archiv : European journal of physiology 391:85–100.

Hamilton NB, Attwell D (2010) Do astrocytes really exocytose neurotransmitters? Nature reviews Neuroscience 11:227–238.

Henson M a, Roberts AC, Pérez-Otaño I, Philpot BD (2010) Influence of the NR3A subunit on NMDA receptor functions. Progress in neurobiology 91:23–37.

Hetman M, Kharebava G (2006) Survival signaling pathways activated by NMDA receptors. Current topics in medicinal chemistry 6:787–799.

Higuchi T, Takeda Y, Hashimoto M, Nagano O, Hirakawa M (2002) Dynamic changes in cortical NADH fluorescence and direct current potential in rat focal ischemia: relationship between propagation of recurrent depolarization and growth of the ischemic core. Journal of cerebral blood flow and metabolism : official journal of the International Society of Cerebral Blood Flow and Metabolism 22:71–79.

Holzwarth JA, Gibbons SJ, Brorson JR, Philipson LH, Miller RJ (1994) Glutamate receptor agonists stimulate diverse calcium responses in different types of cultured rat cortical glial cells. The Journal of neuroscience : the official journal of the Society for Neuroscience 14:1879–1891.

Hoyert D, Xu J (2012) Deaths: Preliminary Data for 2011. National Vital Statistics Reports 61.

Chaudhry FA, Lehre KP, Van Lookeren Campagne M, Ottersen OP, Danbolt NC, Storm-Mathisen J (1995) Glutamate transporters in glial plasma membranes: highly differentiated localizations revealed by quantitative ultrastructural immunocytochemistry. Neuron 15:711–720.

Isokawa M, McKhann GM (2005) Electrophysiological and morphological characterization of dentate astrocytes in the hippocampus. Journal of neurobiology 65:125–134.

Kato H, Narita M, Miyatake M, Yajima Y, Suzuki T (2006) Role of neuronal NR2B subunit-containing NMDA receptor-mediated Ca2+ influx and astrocytic activation in cultured mouse cortical neurons and astrocytes. Synapse (New York, NY) 59:10–17.

Kimelberg HK (2005) Astrocytic swelling in cerebral ischemia as a possible cause of injury and target for therapy. Glia 50:389–397.

Kirischuk S, Kettenmann H, Verkhratsky A (1997) Na+/Ca2+ exchanger modulates kainate-triggered Ca2+ signaling in Bergmann glial cells in situ. FASEB journal : official publication of the Federation of American Societies for Experimental Biology 11:566–572.

Kofuji P, Newman EA (2004) Potassium buffering in the central nervous system. Neuroscience 129:1045–1056.

Krebs C, Fernandes HB, Sheldon C, Raymond LA, Baimbridge KG (2003) Functional NMDA receptor subtype 2B is expressed in astrocytes after ischemia in vivo and anoxia in vitro. The Journal of neuroscience : the official journal of the Society for Neuroscience 23:3364–3372.

Kuraoka M, Furuta T, Matsuwaki T, Omatsu T, Ishii Y, Kyuwa S, Yoshikawa Y (2009) Direct experimental occlusion of the distal middle cerebral artery induces high reproducibility of brain ischemia in mice. Experimental animals / Japanese Association for Laboratory Animal Science 58:19–29.

Lalo U, Palygin O, North RA, Verkhratsky A, Pankratov Y (2011a) Age-dependent remodelling of ionotropic signalling in cortical astroglia. Aging cell 10:392–402.

Lalo U, Pankratov Y, Kirchhoff F, North RA, Verkhratsky A (2006) NMDA receptors mediate neuron-to-glia signaling in mouse cortical astrocytes. The Journal of neuroscience : the official journal of the Society for Neuroscience 26:2673–2683.

Lalo U, Pankratov Y, Parpura V, Verkhratsky A (2011b) Ionotropic receptors in neuronal-astroglial signalling: what is the role of “excitable” molecules in non-excitable cells. Biochimica et biophysica acta 1813:992–1002.

Lalo U, Verkhratsky A, Pankratov Y (2011c) Ionotropic ATP receptors in neuronal-glial communication. Seminars in cell & developmental biology 22:220–228.

Latour I, Gee CE, Robitaille R, Lacaille JC (2001) Differential mechanisms of Ca2+ responses in glial cells evoked by exogenous and endogenous glutamate in rat hippocampus. Hippocampus 11:132–145.

Lee M-C, Ting KK, Adams S, Brew BJ, Chung R, Guillemin GJ (2010) Characterisation of the expression of NMDA receptors in human astrocytes. PloS one 5:e14123.

Li P a, Shamloo M, Katsura KI, Smith ML, Siesjö BK (1995) Critical values for plasma glucose in aggravating ischaemic brain damage: correlation to extracellular pH. Neurobiology of disease 2:97–108.

Liu Z, Zhao W, Xu T, Pei D, Peng Y (2010) Alterations of NMDA receptor subunits NR1, NR2A and NR2B mRNA expression and their relationship to apoptosis following transient forebrain ischemia. Brain research 1361:133–139.

Magistretti PJ (2006) Neuron-glia metabolic coupling and plasticity. The Journal of experimental biology 209:2304–2311.

Malenka RC, Nicoll RA (1999) Long-term potentiation--a decade of progress? Science (New York, NY) 285:1870–1874.

Martínez-Turrillas R, Puerta E, Chowdhury D, Marco S, Watanabe M, Aguirre N, Pérez-Otaño I (2012) The NMDA receptor subunit GluN3A protects against 3-nitroproprionic-induced striatal lesions via inhibition of calpain activation. Neurobiology of disease 48:290–298.

McKenna MC (2007) The glutamate-glutamine cycle is not stoichiometric: fates of glutamate in brain. Journal of neuroscience research 85:3347–3358.

Mehta SL, Manhas N, Raghubir R (2007) Molecular targets in cerebral ischemia for developing novel therapeutics. Brain research reviews 54:34–66.

Metea MR, Newman E a (2006) Glial cells dilate and constrict blood vessels: a mechanism of neurovascular coupling. The Journal of neuroscience : the official journal of the Society for Neuroscience 26:2862–2870.

Mitani A, Tanaka K (2003) Functional changes of glial glutamate transporter GLT-1 during ischemia: an in vivo study in the hippocampal CA1 of normal mice and mutant mice lacking GLT-1. The Journal of neuroscience : the official journal of the Society for Neuroscience 23:7176–7182.

Narahashi T (2008) Tetrodotoxin: a brief history. Proceedings of the Japan Academy Series B, Physical and biological sciences 84:147–154.

Nedergaard M, Dirnagl U (2005) Role of glial cells in cerebral ischemia. Glia 50:281–286.

Nedergaard M, Verkhratsky A (2012) Artifact versus reality--how astrocytes contribute to synaptic events. Glia 60:1013–1023.

Nolte C, Matyash M, Pivneva T, Schipke CG, Ohlemeyer C, Hanisch UK, Kirchhoff F, Kettenmann H (2001) GFAP promoter-controlled EGFP-expressing transgenic mice: a tool to visualize astrocytes and astrogliosis in living brain tissue. Glia 33:72–86.

Oberheim NA, Takano T, Han X, He W, Lin JHC, Wang F, Xu Q, Wyatt JD, Pilcher W, Ojemann JG, Ransom BR, Goldman S a, Nedergaard M (2009) Uniquely hominid features of adult human astrocytes. The Journal of neuroscience : the official journal of the Society for Neuroscience 29:3276–3287.

Onténiente B, Rasika S, Benchoua A, Guégan C (2003) Molecular pathways in cerebral ischemia: cues to novel therapeutic strategies. Molecular neurobiology 27:33–72.

Ottersen OP, Laake JH, Reichelt W, Haug FM, Torp R (1996) Ischemic disruption of glutamate homeostasis in brain: quantitative immunocytochemical analyses. Journal of chemical neuroanatomy 12:1–14.

Pachernegg S, Strutz-Seebohm N, Hollmann M (2012) GluN3 subunit-containing NMDA receptors: not just one-trick ponies. Trends in neurosciences 35:240–249.

Palygin O, Lalo U, Pankratov Y (2011) Distinct pharmacological and functional properties of NMDA receptors in mouse cortical astrocytes. British journal of pharmacology 163:1755–1766.

Palygin O, Lalo U, Verkhratsky A, Pankratov Y (2010) Ionotropic NMDA and P2X1/5 receptors mediate synaptically induced Ca2+ signalling in cortical astrocytes. Cell calcium 48:225–231.

Paoletti P, Neyton J (2007) NMDA receptor subunits: function and pharmacology. Current opinion in pharmacology 7:39–47.

Parpura V, Verkhratsky A (2013) Astroglial amino acid-based transmitter receptors. Amino acids.

Pekny M, Nilsson M (2005) Astrocyte activation and reactive gliosis. Glia 50:427–434.

Pekny M, Pekna M (2004) Astrocyte intermediate filaments in CNS pathologies and regeneration. The Journal of pathology 204:428–437.

Pellerin L, Bouzier-Sore A-K, Aubert A, Serres S, Merle M, Costalat R, Magistretti PJ (2007) Activity-dependent regulation of energy metabolism by astrocytes: an update. Glia 55:1251–1262.

Peterson BL, Park TJ, Larson J (2012) Adult naked mole-rat brain retains the NMDA receptor subunit GluN2D associated with hypoxia tolerance in neonatal mammals. Neuroscience letters 506:342–345.

Phillis JW, Smith-Barbour M, O'Regan MH (1996) Changes in extracellular amino acid neurotransmitters and purines during and following ischemias of different durations in the rat cerebral cortex. Neurochemistry international 29:115–120.

Pivonkova H, Benesova J, Butenko O, Chvatal A, Anderova M (2010) Impact of global cerebral ischemia on K+ channel expression and membrane properties of glial cells in the rat hippocampus. Neurochemistry International 57:783–794.

Rao VL, Dogan A, Todd KG, Bowen KK, Kim BT, Rothstein JD, Dempsey RJ (2001) Antisense knockdown of the glial glutamate transporter GLT-1, but not the neuronal glutamate transporter EAAC1, exacerbates transient focal cerebral ischemia-induced neuronal damage in rat brain. The Journal of neuroscience : the official journal of the Society for Neuroscience 21:1876–1883.

Rossi DJ, Brady JD, Mohr C (2007) Astrocyte metabolism and signaling during brain ischemia. Nature neuroscience 10:1377–1386.

Roy CS, Sherrington CS (1890) On the Regulation of the Blood-supply of the Brain. The Journal of physiology 11:85–158.17.

Scemes E, Giaume C (2006) Astrocyte calcium waves: what they are and what they do. Glia 725:716–725.

Seifert G, Schilling K, Steinhäuser C (2006) Astrocyte dysfunction in neurological disorders: a molecular perspective. Nature reviews Neuroscience 7:194–206.

Seifert G, Steinhäuser C (2001) Ionotropic glutamate receptors in astrocytes. Progress in brain research 132:287–299.

Seki Y, Feustel PJ, Keller RW, Tranmer BI, Kimelberg HK, Robinson SE (1999) Inhibition of Ischemia-Induced Glutamate Release in Rat Striatum by Dihydrokinate and an Anion Channel Blocker Editorial Comment. Stroke 30:433–440.

Schipke CG, Ohlemeyer C, Matyash M, Nolte C, Kettenmann H, Kirchhoff F (2001) Astrocytes of the mouse neocortex express functional N-methyl-D-aspartate receptors. FASEB journal : official publication of the Federation of American Societies for Experimental Biology 15:1270–1272.

Silver I a, Deas J, Erecińska M (1997) Ion homeostasis in brain cells: differences in intracellular ion responses to energy limitation between cultured neurons and glial cells. Neuroscience 78:589–601.

Simard M, Nedergaard M (2004) The neurobiology of glia in the context of water and ion homeostasis. Neuroscience 129:877–896.

Sobolevsky AI, Rosconi MP, Gouaux E (2009) X-ray structure, symmetry and mechanism of an AMPA-subtype glutamate receptor. Nature 462:745–756.

Sofroniew M V (2009) Molecular dissection of reactive astrogliosis and glial scar formation. Trends in neurosciences 32:638–647.

Sofroniew M V, Vinters H V (2010) Astrocytes: biology and pathology. Acta neuropathologica 119:7–35.

Sun L, Kuroiwa T, Ishibashi S, Katsumata N, Endo S, Mizusawa H (2006) Transition of areas of eosinophilic neurons and reactive astrocytes to delayed cortical infarcts after transient unilateral forebrain ischemia in Mongolian gerbils. Acta neuropathologica 111:21–28.

Sun W, McConnell E, Pare J-F, Xu Q, Chen M, Peng W, Lovatt D, Han X, Smith Y, Nedergaard M (2013) Glutamate-Dependent Neuroglial Calcium Signaling Differs Between Young and Adult Brain. Science 339:197–200.

Ventura R, Harris KM (1999) Three-dimensional relationships between hippocampal synapses and astrocytes. The Journal of neuroscience : the official journal of the Society for Neuroscience 19:6897–6906.

Verkhratsky a, Steinhäuser C (2000) Ion channels in glial cells. Brain research Brain research reviews 32:380–412.

Verkhratsky A, Butt A (2007) Glial Neurobiology. Wiley-Interscience.

Verkhratsky A, Rodríguez JJ, Parpura V (2012) Calcium signalling in astroglia. Molecular and cellular endocrinology 353:45–56.

Walz W (2000) Controversy surrounding the existence of discrete functional classes of astrocytes in adult gray matter. Glia 31:95–103.

Wilhelmsson U, Bushong E a, Price DL, Smarr BL, Phung V, Terada M, Ellisman MH, Pekny M (2006) Redefining the concept of reactive astrocytes as cells

that remain within their unique domains upon reaction to injury. Proceedings of the National Academy of Sciences of the United States of America 103:17513–17518.

Won SJ, Kim DY, Gwag BJ (2002) Cellular and molecular pathways of ischemic neuronal death. Journal of biochemistry and molecular biology 35:67–86.

Wu Y, Zhang A-Q, Yew DT (2005) Age related changes of various markers of astrocytes in senescence-accelerated mice hippocampus. Neurochemistry international 46:565–574.

Xie M, Wang W, Kimelberg HK, Zhou M (2008) Oxygen and glucose deprivation-induced changes in astrocyte membrane potential and their underlying mechanisms in acute rat hippocampal slices. Journal of cerebral blood flow and metabolism : official journal of the International Society of Cerebral Blood Flow and Metabolism 28:456–467.

Ye Z-C, Wyeth MS, Baltan-Tekkok S, Ransom BR (2003) Functional hemichannels in astrocytes: a novel mechanism of glutamate release. The Journal of neuroscience : the official journal of the Society for Neuroscience 23:3588–3596.

Zhang Q, Hu B, Sun S, Tong E (2003) Induction of increased intracellular calcium in astrocytes by glutamate through activating NMDA and AMPA receptors. Journal of Huazhong University of Science and Technology Medical sciences = Hua zhong ke ji da xue xue bao Yi xue Ying De wen ban = Huazhong keji daxue xuebao Yixue Yingdewen ban 23:254–257.

Zhou Y, Li HL, Zhao R, Yang LT, Dong Y, Yue X, Ma YY, Wang Z, Chen J, Cui CL, Yu AC-H (2010) Astrocytes express N-methyl-D-aspartate receptor subunits in development, ischemia and post-ischemia. Neurochemical research 35:2124–2134.